Asymptotic formulation of the nonlinear bifurcation scenarios in thermomechanically coupled plates

Noname manuscript No.
(will be inserted by the editor)

Asymptotic formulation of the nonlinear bifurcation scenarios in thermomechanically coupled plates

Valeria Settimi · Giuseppe Rega

the date of receipt and acceptance should be inserted later

Abstract The nonlinear dynamics of composite plates with thermomechanical coupling is analytically addressed in order to describe the main bifurcation phenomena triggering the involved pre- and post-buckling response scenario. The static buckling occurrence, and two resonance conditions around the unbuckled and buckled equilibria are investigated by means of the asymptotic multiple scale method, together with the double-zero bifurcation marking the occurrence of dynamical buckling. The resulting modulation equations and the steady state mechanical and thermal responses are determined and compared with the numerical outcomes in order to verify the adequacy and effectiveness of the refined scalings adopted in the multiple scale analyses to describe the various bifurcation scenarios.

Keywords Laminated plate · Thermomechanical coupling · Nonlinear dynamics · Multiple scale method · Stability and bifurcation · Mechanical buckling

1 Introduction

The nonlinear dynamical behavior of composite plates in a thermomechanical framework is a topic of practical interest in a variety of applications, mostly in aerospace [1], but also in mechanical and civil engineering, as well as in micro-electro-mechanics. As concerns thermomechanical modeling of structures, partially (or one-way) coupled [2–12] as well as fully (or two-way) coupled [13–20] formulations have been proposed in the literature. The former neglect the interaction between mechanical and thermal variables, thus considering an assumed or independently derived temperature distribution to be included into the mechanical

Valeria Settimi
Department of Civil and Building Engineering, and Architecture, Polytechnic University of Marche, 60131 Ancona, Italy
E-mail: v.settimi@staff.univpm.it

Giuseppe Rega
Department of Structural and Geotechnical Engineering, Sapienza University of Rome, 00194 Rome, Italy
E-mail: giuseppe.rega@uniroma1.it

response as known terms involving temperature effects. Conversely, the fully coupled models deal at one time with temperature and displacement variables, so that the thermal energy equation is coupled with the governing mechanical equations via the presence of additional mechanical terms, in a mathematically inseparable context. Although being certainly more involved from a computational viewpoint, the fully coupled models are able to take the actual thermomechanical interaction into account, which can be crucial for catching meaningful effects at both material and structure levels.

When dealing with the nonlinear dynamic behavior of thermomechanical plates, various models of different order and richness have been proposed in the literature, mostly using finite element approaches [6–10]. However, the inherent complexity of these numerical analyses may meaningfully affect a correct interpretation of the nonlinear phenomena. Conversely, resorting to reduced order models which preserve the main features of the underlying continuum formulations may prove essential to pursue easier analyses and a deeper understanding of the basic, yet possibly involved, effects of coupling on the finite amplitude vibrations of geometrically nonlinear structures.

In this framework, two different 2D models of laminated plates with von Kármán nonlinearities have been proposed in the literature, by either neglecting [21] or considering [22] shear deformability, and by consistently assuming a corresponding linear or cubic variation of the unknown thermal field along the plate thickness. For symmetric cross-ply laminates, a proper and controllable dimension reduction accomplished via Galerkin approximations has allowed in both cases to end up to a minimal model (with one mechanical and two thermal equations/unknowns) still exhibiting the fundamental features of geometrical nonlinearity and thermomechanical coupling embedded in the underlying continuum models. A systematic numerical investigation of the general nonlinear features of local and global response has allowed the authors to discuss the system response to different thermal boundary conditions possibly included in the model formulation, as well as to mechanical and thermal external excitations. The outcomes have highlighted the transition to mechanically- or thermally-induced buckled responses [23, 24], with also a focus on the different role played by coupling terms in different excitation conditions [25]. Furthermore, global dynamics has shown to be of major importance for reliably catching the non-trivial influence of the slow transient thermal dynamics on the steady outcome of the faster mechanical response [26].

Overall, the nonlinear behavior of the thermomechanical plate turns out to be characterized by a rich and involved scenario with multistability regions and chaotic solutions, whose description can be only achieved by means of refined numerical tools. Yet, unveiling and analyzing the essential dynamical phenomena underlying the system response can be crucial for a deep understanding of the nonlinear dynamics of reduced order models. Indeed, the use of analytical asymptotic approaches, such as the multiple time scale method [27], can allow to shed light on the often disordered and abundant results provided by numerical investigations [28], and to predict, describe, and potentially modify the behavior of the coupled system.

Actually, to the best of the authors' knowledge, the effective use of multiple scales for dealing with coupled thermomechanical problems is still quite limited; see, e.g., the analysis of nonlinear dynamics and bifurcations of coupled thermo-

optical MEMS oscillators in [29]. Indeed, due to the multiphysics nature of the involved models, the two-field different effects ensuing from the concurrent presence of fast mechanical and slow thermal dynamical evolutions, and also consisting of different roles played by the coupling terms in the mechanical and thermal responses, need to be correctly contemplated in order to properly define the perturbation procedures. This being an issue that has recently been addressed also in the general framework of a possibly systematic and efficient reduction of temperature dependent equations of structural dynamics, where a multiple scale approach may allow to consistently account for the coexisting slow/fast thermo/mechanical settings [30].

In this framework, the dynamics of the previously obtained reduced model of shear deformable thermomechanical plate with cubic temperature variation along the plate thickness [22], is herein analyzed in weakly nonlinear regime under mechanical excitations, with three main dynamical phenomena being detected. In order to investigate each of them by means of the asymptotic multiple scale method, hints obtained from the previous numerical analyses are properly implemented. Analytical procedures with different scaling of the variables and parameters, as well as different orders of development, are presented, and the existence and stability of mechanical and thermal responses are discussed.

The paper is organized as follows. In Section 2, the thermomechanical plate model is summarized, with the main assumptions in the background and the reduced order equations of motion. An illustrative behavior of the system response in strongly nonlinear regime is also described, along with the identification of the essential dynamical phenomena. The following three sections analyze the asymptotic primary resonant response of the model in pre-buckling (Sect. 3) and post-buckling (Sect. 4) conditions, as well as the double-zero bifurcation marking the boundary in between them (Sect. 5). All the involved analytical treatments are presented in corresponding Appendices. Comparisons of analytical predictions with numerical outcomes are also accomplished for the three considered cases. Eventually, concluding remarks are reported in Sect. 6.

2 Model and dynamical response

The model under analysis is represented by a rectangular laminated plate with von Kármán nonlinearities, third-order shear deformability, and consistent cubic variation of the temperature along the thickness, whose formulation is presented in [22], to refer to for all details. Furthermore, the relevant dimensionless model has been adopted in [23–26], where nondimensionalization with respect to time, plate thickness, and external frequency has been assumed in order to numerically investigate the nonlinear dynamical response just at primary resonance. To apply an asymptotic approach requiring the explicitation of the forcing frequency, nondimensionalization with respect to the system mechanical natural frequency is adopted herein. Accordingly, and assuming isothermal edges and free heat exchange on the upper and lower surfaces, the following three coupled dimensionless ordinary differential equations (ODEs) of motion describing the plate dynamics

are obtained:

$$\begin{aligned}
&\ddot{W} + a_{12}\dot{W} + (1-p)W + a_{14}W^3 + a_{15}T_{R1} + a_{16}T_{R0}W - f\cos\Omega t = 0 \\
&\dot{T}_{R0} + a_{22}T_{R0} + a_{23}\alpha_1 T_\infty + a_{24}W\dot{W} = 0 \\
&\dot{T}_{R1} + a_{32}T_{R0} + a_{33}\dot{W} = 0
\end{aligned} \tag{1}$$

in terms of the nondimensional reduced variables $W(t)$ (deflection of the center of the plate), $T_{R0}(t)$ (membrane temperature) and $T_{R1}(t)$ (bending temperature). The nondimensional mechanical excitations consist of a uniform steady in-plane compressive force p on the plate edges, and a distributed harmonic transverse mechanical excitation of amplitude f and frequency Ω. The thermal boundary condition included in the membrane temperature equation is assumed to represent a free heat exchange between the plate and the environment, with the relevant constant thermal difference being represented by the parameter T_∞. Coefficients a_{ij} incorporate the geometrical and physical properties of the model, and the numerical values selected to develop the following numerical investigations are reported in Appendix A.

The interaction terms between mechanical and thermal variables are present in all equations and highlight a full thermomechanical coupling. Although the model is formulated to include different kinds of (body and/or boundary) thermal excitations [22], in the following analyses the sole boundary thermal condition is considered, together with the purely mechanical excitations.

The numerical dynamical behavior of the plate in strongly nonlinear regime at primary external resonance has been the subject of previous publications [23–26], which have already shown a quite rich and involved scenario with multistable regions and also chaotic responses. In particular, bifurcation diagrams of the three variables as a function of mechanical precompression p and thermal boundary condition T_∞ are reported in Fig. 1. Both parameters have been shown to play a role in modifying the mechanical linear stiffness due to the thermomechanical coupling inside the mechanical equation. Indeed, they produce the same effect on the mechanical and bending thermal variables, so that it is possible to reproduce exactly the diagrams of Fig. 1(a),(b) by alternatively applying a properly scaled thermal excitation or a mechanical precompression. Differently, the membrane temperature, which is directly activated by the thermal boundary condition, exhibits different responses, as shown in Fig. 1(c). In general, the diagrams highlight the transition to mechanically- or thermally-induced buckled responses, with the passage from a monostable dynamics for low values of the parameters, to a rich multistable behavior in the high values region.

The bifurcation diagrams are realized by means of the software AUTO [31] plotting, for each branch, the maximum and minimum values of the relevant variable, so that it is immediate to verify not only the stability range of each solution, but also its amplitude. Accordingly, in the multistable region, a variety of 1-period solutions can be detected, with a couple of low-amplitude buckled responses (orange $\mathrm{P1^{I}}$/red $\mathrm{P1^{II}}$) and a couple of high-amplitude buckled solutions (cyan $\mathrm{P1^{III}}$/blue $\mathrm{P1^{IV}}$), coexisting with the gray P1 solution. The latter represents the sole solution existing in the pre-buckling regime, while in the post-buckling region it becomes a cross-well response oscillating around both varied equilibria.

In the light of these results, the objective of the present work is to unveil the bifurcation phenomena triggering the development of this rich multistable

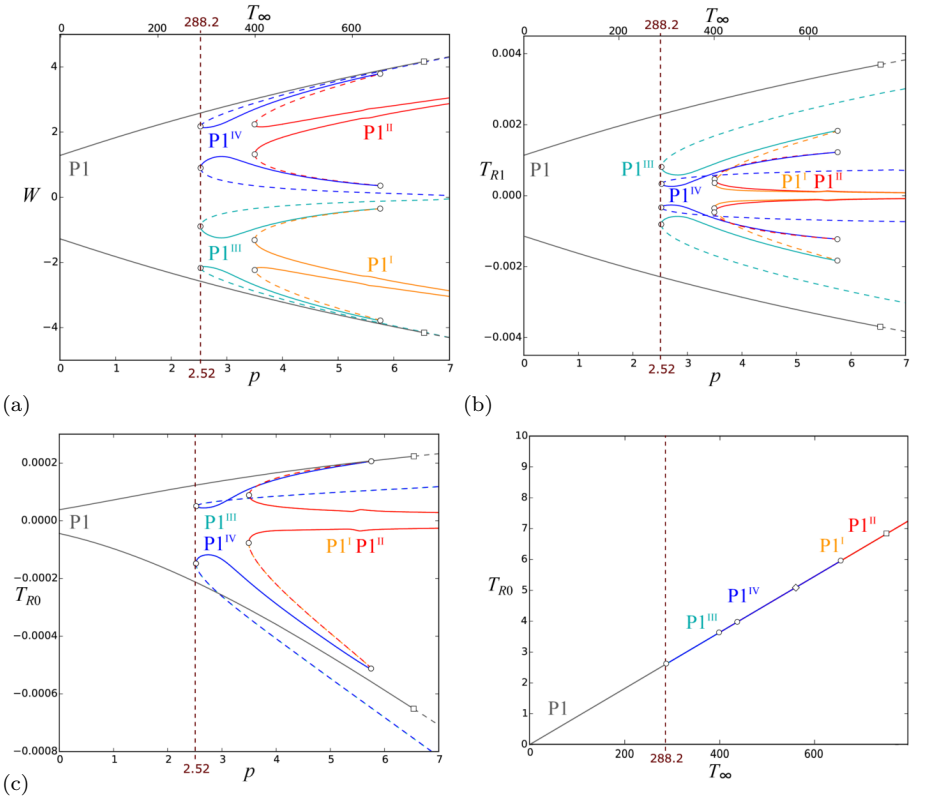

Fig. 1 For $\Omega = 1$ and $f = 1$, bifurcation diagrams of mechanical displacement W (a), bending temperature T_{R1} (b) and membrane temperature T_{R0} (c) as a function of mechanical precompression p and thermal variation T_∞. Circle: saddle-node bifurcation; Square: transcritical bifurcation; Diamond: period-doubling bifurcation. (Color figure online)

scenario and to comprehensively investigate it via an asymptotic approach. To this aim, several bifurcation diagrams are obtained in the weakly nonlinear regime by lowering the forcing amplitude of the mechanical excitation in order to follow the evolution of the stable branches. One example is reported in Fig. 2, where the forcing amplitude is one tenth of the value previously considered. From the diagram, it can be observed that the six 1-period solutions are associated with four main phenomena, namely: (i) A static pitchfork bifurcation inducing the mechanical buckling, when the mechanical precompression p nullifies the linear mechanical stiffness; (ii) a primary resonance involving the pre-buckling branch; (iii-iv) a primary resonance at each of the two symmetric post-buckling branches.

Hence, as first analysis, the static equilibria of the coupled system (1) are analytically determined as follows, by solving the relevant undamped unforced

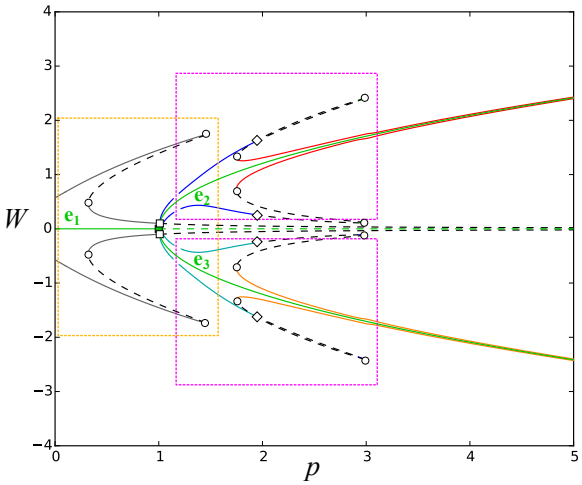

Fig. 2 For $\Omega = 1$, $T_\infty = 0$ and $f = 0.1$, bifurcation diagram of mechanical displacement W as a function of mechanical precompression p. Circle: saddle-node bifurcation; Square: pitchfork bifurcation; Diamond: period-doubling bifurcation. Green diagram: static buckling; yellow-squared region: primary resonance around pre-buckling equilibrium; magenta-squared regions: primary resonance around post-buckling equilibria. (Color figure online)

model:

$$\begin{aligned}
&\mathbf{e_1} = \{W_{e_1}, T_{R0e_1}, T_{R1e_1}\} = \{0, -\frac{a_{23}\alpha_1 T_\infty}{a_{22}}, 0\},\\
&\mathbf{e_{2,3}} = \{W_{e_{2,3}}, T_{R0e_{2,3}}, T_{R1e_{2,3}}\} = \{\pm\frac{\sqrt{a_{22}(p-1)+a_{16}a_{23}\alpha_1 T_\infty}}{\sqrt{a_{14}a_{22}}}, -\frac{a_{23}\alpha_1 T_\infty}{a_{22}}, 0\}
\end{aligned} \tag{2}$$

The $\mathbf{e_1}$ equilibrium corresponds to the pre-buckling configuration representing the mechanical rest position, while $\mathbf{e_2}$ and $\mathbf{e_3}$ represent the two stable buckled non-trivial solutions arising from the pitchfork bifurcation. The $p - T_\infty$ relation describing the buckling condition, i.e. the static pitchfork bifurcation equation, is readily obtained as:

$$p = -\frac{\alpha_1 a_{16} a_{23} T_\infty}{a_{22}} + 1 \tag{3}$$

The subsequent investigation of the resonance conditions is then developed by studying the weakly nonlinear dynamics around the detected equilibria. Due to the symmetry of the buckled branches, the analysis will be focused only on the positive buckled equilibrium.

3 Primary resonance around pre-buckling equilibrium

The weakly nonlinear dynamics analysis is accomplished by means of the asymptotic Multiple Scale Method [27] in order to study the system response around the $\mathbf{e_1}$ equilibrium: $W(t) = W_{e_1} + \tilde{W}$, $T_{R0}(t) = T_{R0e_1} + \tilde{T}_{R0}$, $T_{R1}(t) = T_{R1e_1} + \tilde{T}_{R1}$.

Accordingly, the system equations read:

$$\begin{aligned}
&\ddot{\tilde{W}} + a_{12}\dot{\tilde{W}} + \omega^2\tilde{W} + a_{14}\tilde{W}^3 + a_{15}\tilde{T}_{R1} + a_{16}\tilde{T}_{R0}\tilde{W} - f\cos\Omega t = 0 \\
&\dot{\tilde{T}}_{R0} + a_{22}\tilde{T}_{R0} + a_{24}\tilde{W}\dot{\tilde{W}} = 0 \\
&\dot{\tilde{T}}_{R1} + a_{32}\tilde{T}_{R0} + a_{33}\dot{\tilde{W}} = 0
\end{aligned} \tag{4}$$

where the coefficient ω^2 of the linear mechanical stiffness is defined as

$$\omega^2 = 1 - p - \frac{a_{16}a_{23}\alpha_1 T_\infty}{a_{22}} \tag{5}$$

It is worth noting that the term related to the thermal boundary condition T_∞ in the membrane equation of system (1) in not present in (4). Indeed, it is a time-independent term which influences the membrane temperature of equilibrium $\mathbf{e_1}$; however, due to the ensuing thermal coupling inside the mechanical equation, it is also able to modify the linear mechanical stiffness, as shown in Eq. (5).

Due to the presence of only cubic nonlinear term in the mechanical equation (4), three time scales have been introduced, i.e., $T_0 = t$, $T_1 = \epsilon t$, $T_2 = \epsilon^2 t$, where ϵ is a small dimensionless ordering parameter. Moreover, primary resonance is investigated by imposing $\omega^2 = \Omega^2 + \epsilon\,\sigma$, with σ being the detuning parameter.

In order to properly scale system variables and parameters, useful information can be obtained from the numerical analyses of the nonlinear response [26]. In fact, several outcomes in local and global dynamics have pointed out the different time scales on which thermal (slow) and mechanical (fast) dynamics evolve, with the thermal transient being very long with respect to the mechanical one. This behavior is typical for systems with multiphysics coupling, and strongly modifies the mechanical steady response of the coupled system with respect to an uncoupled model. Furthermore, detailed numerical investigations have allowed us to discuss the role of the coupling terms inside the three equations [25]. They result to be crucial into the thermal equations in order to determine the temperature response [32], while having a marginal effect on the mechanical equation, whose dynamics evolves much quicker than the coupled thermal one. For the purposes of the present work, this behavior suggests to associate the thermal variables to a time scale different from that of the mechanical variable in the multiple scale approach. Moreover, coupling terms into thermal equations should appear at lower orders than those into the mechanical equation, in order to properly describe the slower thermal evolution.

Accordingly, variables and parameters are properly scaled to obtain the following perturbation scheme:

- Order ϵ **Mechanical equation:** linear stiffness (generating solution)
- Order ϵ^2 **Mechanical equation:** cubic term, damping, excitation, detuning
  Thermal equations: mechanical coupling terms (a_{24}, a_{33})
- Order ϵ^3 **Mechanical equation:** thermal coupling terms (a_{15}, a_{16})

Details about the asymptotic procedure are reported in Appendix B. The following amplitude modulation equations (AMEs) for the mechanical amplitude in

polar form result

$$\begin{aligned}\dot{a} &= 2(c_{11i}\sin\theta + c_{1r}\cos\theta) + c_{21r}a - \frac{3}{2}c_{3i}a^2\sin\theta + \frac{c_{4r}}{4}a^3 \\ a\dot{\theta} &= 2(c_{11i}\cos\theta - c_{1r}\sin\theta) + c_{21i}a - \frac{1}{2}c_{3i}a^2\cos\theta + \frac{c_{41i}}{4}a^3 + \frac{c_{5i}}{16}a^5\end{aligned} \tag{6}$$

while the reconstructed solutions read

$$\begin{aligned}W(t) &= W_{e_1} + \tilde{W} = a\cos\psi + c_6\, a^3\cos(3\psi) \\ T_{R0}(t) &= T_{R0e_1} + \tilde{T}_{R0} = T_{R0e_1} + c_7\, a^2\cos(2\psi) + c_8\, a^2\sin(2\psi) \\ T_{R1}(t) &= T_{R1e_1} + \tilde{T}_{R1} = c_9\, a\cos\psi + c_{10}\, a\sin\psi\end{aligned} \tag{7}$$

where a and θ are the real amplitude and phase of the mechanical response, respectively, $\psi = \Omega t + \theta$, and the expressions of c_{jk} and c_{j1k} $(k = i, r)$ coefficients are reported in Appendix B.

It is worth highlighting that mechanical and thermal excitations represented by p and T_∞, respectively, are taken into account into the asymptotic equations by the detuning parameter σ, through Equation (5). In turn, σ is included in the coefficients $c_{11i} = c_{11i}(\sigma)$, $c_{21i} = c_{21i}(\sigma, \sigma^2)$, $c_{41i} = c_{41i}(\sigma)$. This means that the excitations modify constant, linear and cubic terms into the modulation equations. As concerns the reconstructed solutions, the mechanical response is a combination of harmonic and order-3 superharmonic contributions, while the thermal solutions are obtained as single-contribution responses. In particular, membrane response is order-2 superharmonic due to the quadratic nature of the mechanical coupling $a_{24}W\dot{W}$ into the membrane thermal equation, while bending temperature has only harmonic contributions due to the linear coupling with mechanical response through the $a_{33}\dot{W}$ term into the bending thermal equation.

To analytically determine the nonlinear mechanical frequency, the undamped unforced amplitude modulation equations (6) are obtained by nullifying the forcing and damping coefficients of Eqs. (4), i.e. $a_{12} = f = a_{24} = a_{33} = 0$. The resulting equations are:

$$\begin{aligned}\dot{a} &= 0 \\ a\dot{\theta} &= c_{21i}a + \frac{c_{41i}}{4}a^3 + \frac{c_{5i}}{16}a^5\end{aligned} \tag{8}$$

The former equation states that the amplitude is time-independent, while integration of the latter furnishes the phase angle θ linearly depending on time according to the function

$$\theta(t) = \theta_0 + \varpi t, \qquad \varpi = \left(c_{21i} + \frac{c_{41i}}{4}a^2 + \frac{c_{5i}}{16}a^4\right) \tag{9}$$

where ϖ represents the amplitude-dependent nonlinear mechanical frequency.

Validation of the asymptotic procedure is performed by comparing the analytical results obtained for the three variables of the thermomechanical problem (red curves) with the outcomes from numerical integration of system ODEs (1) (black curves), in terms of response diagrams versus the varying bifurcation parameter (p or T_∞) (Fig.3) and of periodic solutions in the state planes (Fig.4). The analytical results from Eqs. (6) and (7) are obtained by means of Mathematica [33]. As regards the bifurcation diagrams of Fig.3, the real asymptotic mechanical

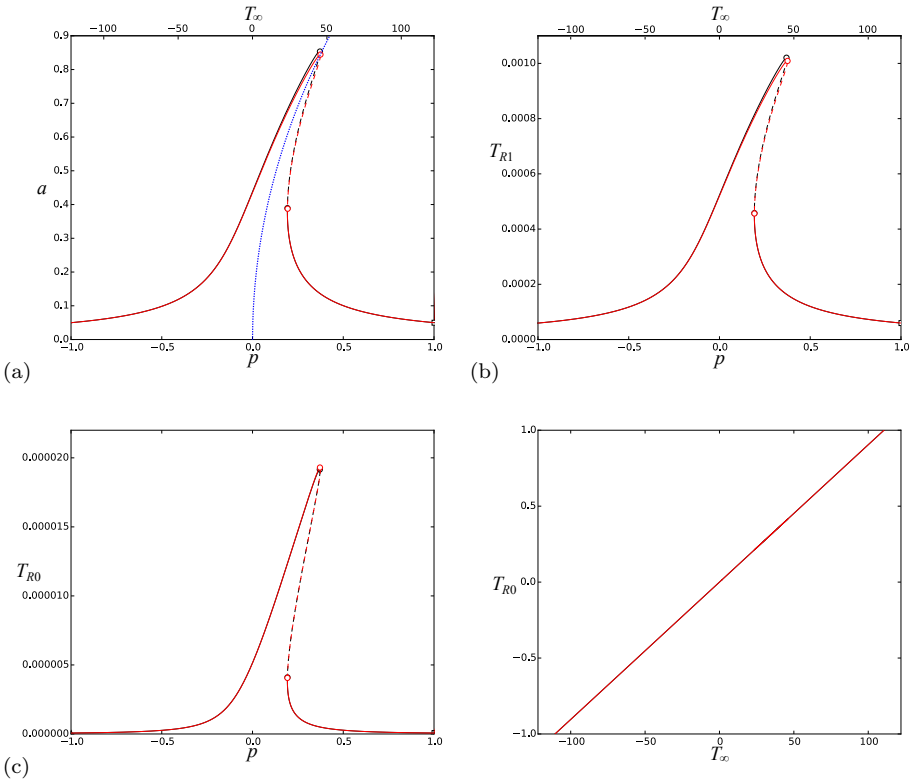

Fig. 3 For $\Omega = 1$ and $f = 0.05$, comparison between numerical (black) and asymptotic (red) responses for mechanical amplitude a (a), bending temperature T_{R1} (b) and membrane temperature T_{R0} (c). Precompression p or, alternatively, thermal difference T_∞ is assumed as bifurcation parameter.
The blue dashed curve in (a) represents the analytical backbone curve. Circle: saddle-node bifurcation.(Color figure online)

amplitude from (6) is compared with the numerical amplitude obtained as semi-difference between the maximum and minimum values of the periodic response: $a_{\text{num}} = (\max(W) - \min(W))/2$. Note that in this way the static component of the numerical response (which in this case is actually vanishing) is filtered out. Differently, the maximum numerical oscillation of each thermal variable is compared with the corresponding maximum asymptotic value furnished by the reconstructed solutions (7). The asymptotic (red) and numerical (black) diagrams completely overlap for all variables. Thus, the proposed perturbation procedure proves capable of almost perfectly reproducing the behavior of the system, both around and outside the resonance region, also when the response amplitudes reach moderately severe values in the resonance peak. Moreover, the nonlinear mechanical frequency (9) has been plotted to obtain the analytical backbone curve (blue dashed curve in Fig.3(a)) which is able to accurately reproduce the trend of the resonance curve.

It is worth highlighting that the proposed asymptotic treatment holds not only for variations of the mechanical prestress, but also for the possible presence of a

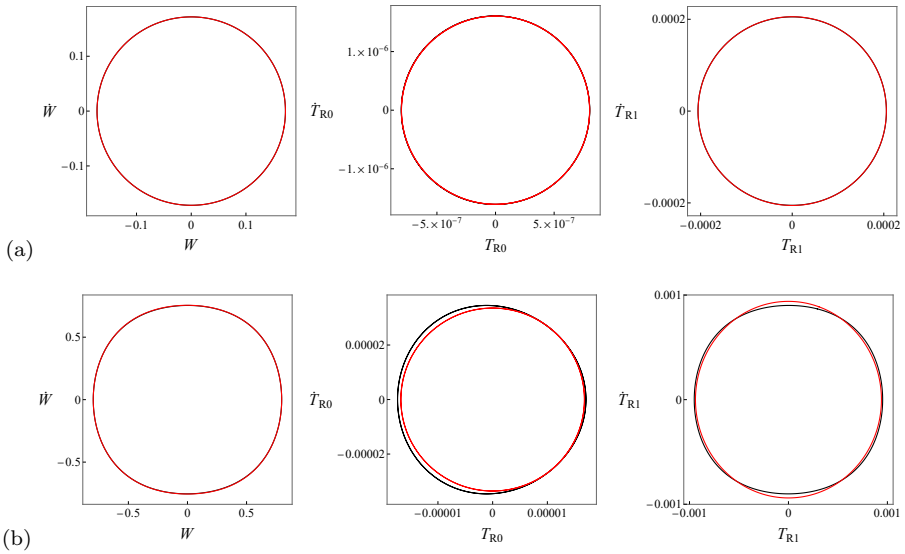

Fig. 4 For $\Omega = 1$ and $f = 0.05$, $p = 0.3$, low-amplitude (a) and high-amplitude (b) 1-period solutions in the mechanical and thermal state planes. Black curves: numerical response; red curves: asymptotic response. (Color figure online)

temperature difference between plate and environment. Indeed, figure 3 confirms that, also in the analytical treatment, p and T_∞ produce equivalent effects in terms of mechanical displacement W and bending temperature T_{R1}, while the thermal variation T_∞ makes the membrane temperature T_{R0} settle onto a straight line, as expected (Fig.3(c), right panel).

Finally, figure 4 shows the ability of the obtained results in perfectly reproducing the low-amplitude nonresonant system response in the mechanical and thermal state planes (Fig.4(a)). However, looking at the high-amplitude resonant solution, the mechanical response is seen to be well reproduced, while the asymptotic thermal solutions exhibit a slight difference with respect to the numerical outcomes (Fig.4(b)). This is due to the fact that a single harmonic contribution has been considered in the thermal solutions (7), without transferring the order-3 superharmonic contribution of the mechanical response into the thermal response. However, the difference is only marginal and concerns the form of the solution rather than its amplitude.

4 Primary resonance around post-buckling equilibrium

The analysis around the buckled $\mathbf{e_2}$ equilibrium ($W(t) = W_{e_2} + \tilde{W}$, $T_{R0}(t) = T_{R0e_2} + \tilde{T}_{R0}$, $T_{R1}(t) = T_{R1e_2} + \tilde{T}_{R1}$) leads to the following set of equations:

$$\begin{aligned}
&\ddot{\tilde{W}} + a_{12}\dot{\tilde{W}} + \omega^2\tilde{W} + a_{14}\tilde{W}^3 + \frac{3}{2a_{141}}\omega\tilde{W}^2 + a_{15}\tilde{T}_{R1} + a_{16}(\omega a_{141} + \tilde{W})\tilde{T}_{R0} - f\cos(\Omega t) = 0\\
&\dot{\tilde{T}}_{R0} + a_{22}\tilde{T}_{R0} + a_{24}\dot{\tilde{W}}(\omega a_{141} + \tilde{W}) = 0\\
&\dot{\tilde{T}}_{R1} + a_{32}\tilde{T}_{R0} + a_{33}\dot{\tilde{W}} = 0
\end{aligned} \tag{10}$$

where

$$\omega^2 = 2\left(p - 1 + \frac{a_{16}a_{23}\alpha_1 T_\infty}{a_{22}}\right), \quad a_{141} = \frac{1}{\sqrt{2a_{14}}} \tag{11}$$

Additional terms in mechanical and membrane thermal equations can be recognized with respect to the pre-buckling analysis. Consequently, the asymptotic procedure in post-buckling regime requires a different scaling of variables and parameters, and different expansions to higher orders are needed to account for the main effects due to the presence of both quadratic and cubic nonlinearities into the mechanical equation. Accordingly, five time scales have been introduced, i.e., $T_0 = t$, $T_1 = \epsilon t$, $T_2 = \epsilon^2 t$, $T_3 = \epsilon^3 t$, $T_4 = \epsilon^4 t$, while primary resonance is investigated by imposing $\omega^2 = \Omega^2 + \epsilon^2\sigma$, with σ being the detuning parameter. Variables and parameters are properly scaled in order to obtain the following perturbation scheme:

- Order ϵ **Mechanical equation:** linear stiffness (generating solution)
- Order ϵ^2 **Mechanical equation:** quadratic term
  Thermal equations: mechanical coupling terms (a_{24}, a_{33})
- Order ϵ^3 **Mechanical equation:** cubic term, damping, excitation, detuning
  Thermal equations: correction
- Order ϵ^4 **Mechanical equation:** thermal coupling terms (a_{15}, a_{16})
  Thermal equations: correction
- Order ϵ^5 **Mechanical equation:** correction

Details about the asymptotic procedure are reported in Appendix C. The following modulation equations for the mechanical amplitude in polar form result

$$\begin{aligned}
\dot{a} &= +2(c_{1i}\sin\theta + c_{1r}\cos\theta) + c_{2r}a + \frac{5c_{3i}a^2\sin\theta}{4} + \frac{c_{4r}a^3}{4}\\
a\dot{\theta} &= 2(c_{1i}\cos\theta - c_{1r}\sin\theta) + c_{2i}a - \frac{c_{3i}a^2\cos\theta}{4} + \frac{c_{4i}a^3}{4} + \frac{c_{5i}a(t)^5}{16}
\end{aligned} \tag{12}$$

while the reconstructed solutions read

$$\begin{aligned}
&W(t) = W_{e_2} + \tilde{W} = W_{e_2} - 3c_6a^2 - 27c_7a^4 + a\cos\psi + c_8a\cos(2\psi-\theta)\\
&+ (c_6a^2 + 14c_7a^4)\cos(2\psi) + c_9a^2\sin(2\psi) + c_{10}a^3\cos(3\psi) + c_7a^4\cos(4\psi)\\
&T_{R0}(t) = T_{R0e_2} + \tilde{T}_{R0} = T_{R0e_2} + c_{11}\cos(\psi-\theta) + c_{12}a\cos\psi + c_{13}a^3\cos\psi\\
&+ c_{14}a^2\cos(2\psi) + c_{15}a^3\cos(3\psi) + c_{16}\sin(\psi-\theta) + c_{17}a\sin\psi + c_{18}a^3\sin\psi\\
&+ c_{19}a^3\sin(3\psi) + c_{20}a^2\sin(2\psi)\\
&T_{R1}(t) = T_{R1e_2} + \tilde{T}_{R0} = c_{21}\cos(\psi-\theta) + c_{22}a\cos\psi + c_{23}a^3\cos\psi\\
&+ c_{24}a^2\cos(2\psi) + c_{25}a^3\cos(3\psi) + c_{26}\sin(\psi-\theta) + c_{27}a\sin\psi\\
&+ c_{28}a^3\sin\psi + c_{29}a^2\sin(2\psi) + c_{30}a^3\sin(3\psi)
\end{aligned} \tag{13}$$

where a and θ are the real amplitude and phase of the mechanical response, respectively, $\psi = \Omega t + \theta$, and the expressions of c_{jk} and c_{j1k} $(k = i, r)$ coefficients are reported in Appendix C. It is worth noting that the obtained AMEs for the mechanical response are formally equal to those obtained from the pre-buckling analysis (6) presented in the previous section, although with different c_{ij} expressions. Differently, the analytical expressions of the mechanical and thermal solutions are enriched by several contributions with respect to the pre-buckling case (7), due to the increased number of perturbation orders here considered.

As for the pre-buckling analysis, the nonlinear mechanical frequency can be analytically determined by studying the undamped unforced amplitude modulation equations (12), which are obtained by nullifying the forcing and damping coefficients in Eqs. (10), i.e. $a_{12} = f = a_{24} = a_{33} = 0$:

$$\begin{aligned}
&\dot{a} = 0\\
&a\dot{\theta} = c_{2i}a + \frac{c_{4i}}{4}a^3 + \frac{c_{5i}}{16}a^5
\end{aligned} \tag{14}$$

Integrating the latter equation allows us to get the amplitude-dependent nonlinear mechanical frequency ϖ, which can be employed to obtain the mechanical backbone curve:

$$\theta(t) = \theta_0 + \varpi t, \qquad \varpi = \left(c_{2i} + \frac{c_{4i}}{4}a^2 + \frac{c_{5i}}{16}a^4\right) \tag{15}$$

Like the amplitude modulation equations, also the nonlinear mechanical frequencies have the same expressions in pre-buckling and post-buckling resonances, with different definitions of the relevant coefficients.

Comparison between numerical (black curves) and analytical (red curves) results is reported in Fig.5 in terms of mechanical and thermal bifurcation diagrams. As in the previous section, the asymptotic mechanical amplitude obtained from the AMEs (12) is compared with the semi-difference of maximum and minimum values of the numerical oscillation from the ODEs (1). Note that also in this case the non-vanishing static component of the overall numerical response is filtered out. Analytical thermal responses are obtained in terms of maximum values of the corresponding reconstructed solutions (13).

Looking at Figs.5(a),(b), a very good agreement between numerical and analytical outcomes can be observed for the mechanical displacement W and the bending temperature T_{R1}. Differently, the asymptotic response of the membrane

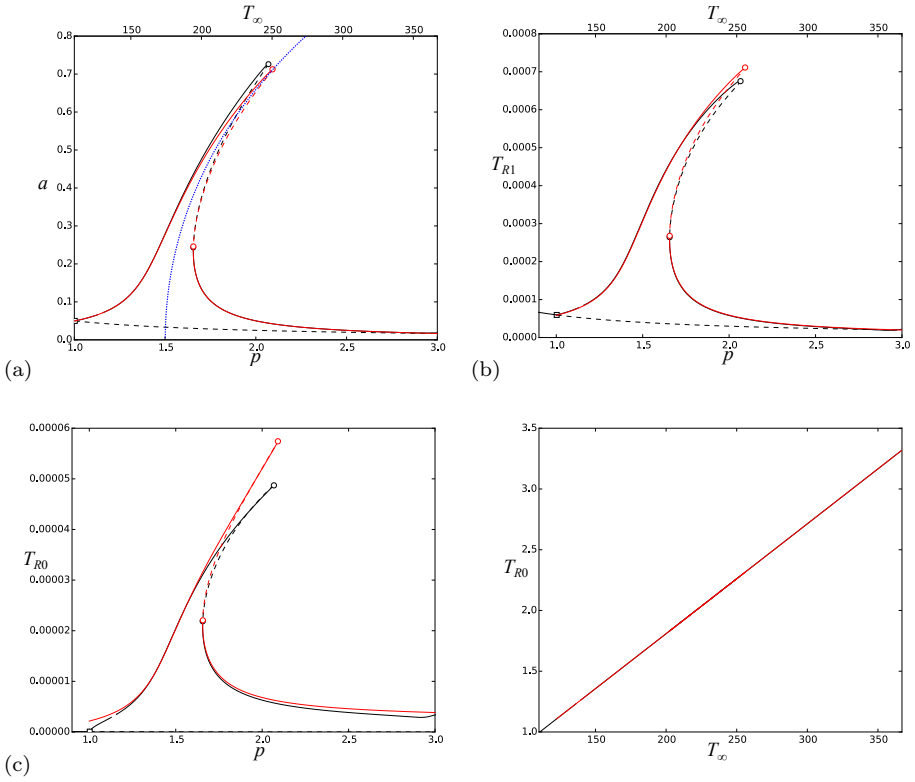

Fig. 5 For $\Omega = 1$ and $f = 0.05$, comparison between numerical (black) and asymptotic (red) responses for mechanical amplitude a (a), bending temperature T_{R1} (b) and membrane temperature T_{R0} (c). Precompression p or, alternatively, thermal difference T_∞ is assumed as bifurcation parameter. The blue dashed curve in (a) represents the analytical backbone curve. Circle: saddle-node bifurcation; square: pitchfork bifurcation. (Color figure online)

temperature T_{R0} for varying precompression p (left panel of Fig.5(c)) is acceptable near the resonance condition, with a slight overestimation of the peak, which is coherent with the trend of the bending temperature (Fig.5(b)), and also with the reconstructed mechanical response (see Fig.9(b) forward). Away from the resonance region, however, the numerical membrane response is not correctly reproduced by the analytical results, especially in the lowest range of p values where the pre- and post-buckling branches should be connected to each other through the pitchfork bifurcation point. Observing the expressions of the analytical solutions in pre- and post-buckling regimes, the pre-buckling membrane response (second of (7)) is seen to be governed by the order-2 superharmonic contribution, coherently with the quadratic nature of the coupling term present in the membrane equation (a_{24} term in (4)). In the post-buckling regime, conversely, the reconstructed membrane response (13) is characterized by several frequency contents, including all harmonic contributions originated by the $a_{24}\omega a_{141}\dot{W}$ term in equation (10), which is absent in the pre-buckling system. Since the asymptotic procedure provides for the imposition of the resonance condition (11) (and relevant square root), such ω-dependent term becomes dominant in the membrane response, not only in the

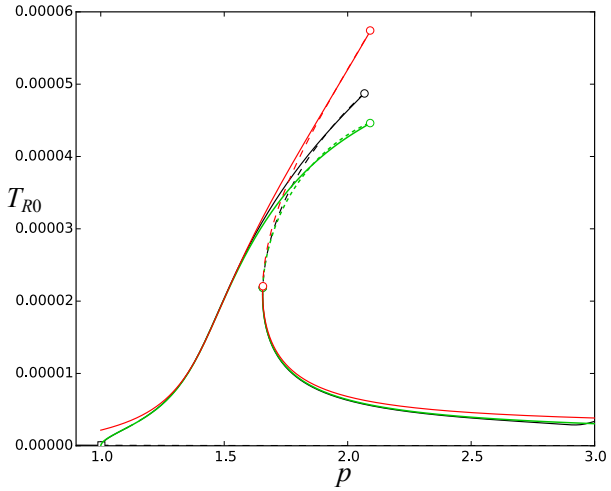

Fig. 6 For $\Omega = 1$ and $f = 0.05$, comparison between numerical response (black), asymptotic response with resonance conditions applied in all terms (red), and asymptotic response with resonance conditions applied only in the purely mechanical terms (green), for the membrane temperature T_{R0}. Circle: saddle-node bifurcation. (Color figure online)

resonance region but also in the nonresonant range and around the bifurcation point. Such observation suggests to asymptotically study the thermal response outside the resonance region by applying the same asymptotic procedure, without however resonating the ω-dependent terms related to the thermal variable. This approach sounds reasonable in physical terms since the thermal solution is not directly forced by the harmonic excitation but is merely dragged into the overall response by the mechanical component.

Therefore, an alternative asymptotic procedure is developed by imposing the resonance condition only to the terms related to W and W^2 in the mechanical equation (10). Following the same scheme previously described allows us to determine the AMEs for the mechanical variable, which turn out to be formally identical to those in (12). The expressions of the c_{ij} coefficients are equal too, apart from a slight difference in the a_{16}-dependent terms of the c_{2r}, c_{2i} coefficients, which anyway have a completely negligible influence on the mechanical response. The bending thermal response is not influenced by the different imposition of the resonance condition, while the analytical membrane temperature, which is formally identical to (13), shows different expressions of the coefficients (see Eq. (70) in Appendix C). The behavior of the resulting membrane thermal response is described by the green curve of Fig.6, which is compared with the previous analytical results (red curve) and with the ODEs numerical integration (black curve). The new asymptotic solution is able to correctly reproduce the numerical outcomes even far from the resonance region, while the resonance peak is slightly underestimated due to the minor contribution provided by the dragging harmonic component which dominates the (mechanical) response in this region.

The post-buckling solutions in the mechanical and thermal phase planes are reported in Fig.7 and confirm the goodness of the overall asymptotic approach

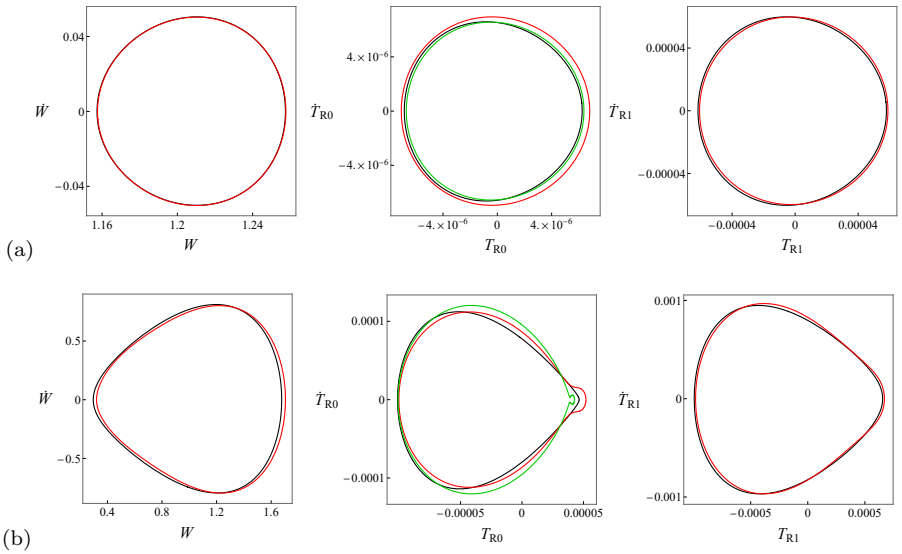

Fig. 7 For $\Omega = 1$, $f = 0.05$, $p = 2.0$, low-amplitude (a) and high-amplitude (b) 1-period solutions in the mechanical and thermal state planes. Black curves: numerical response; red curves: asymptotic response with resonance conditions applied in all terms; green curves: asymptotic response with resonance conditions applied only to the purely mechanical terms. (Color figure online)

for both resonant and nonresonant responses. It is worth underlining that the symmetry distortion effect in the shape of the resonant mechanical response, now entailed by the even superharmonic contributions also present in the analytical solution with respect to the pre-buckling one, is fully consistent with the numerical outcome. As regards the membrane thermal response, the nonresonant solution is slightly overestimated by the asymptotic procedure with resonance in all ω-dependent terms (red curve), while it is correctly reproduced by the asymptotic approach without resonance in the ω-dependent terms related to the thermal variable (green curve). However, as far as the resonant solution is concerned, the latter approach not only slightly underestimates the response amplitude, as already seen before in Fig.6, but it also worse reproduces the overall form of the numerical solution, which is evidently influenced by the order-1 and order-3 contributions provided by the mechanical variable. Conversely, the red response, with resonance in all terms, proves to better fit the numerical solution in the resonant case.

5 Asymptotic analysis of double-zero bifurcation

In order to properly define the range of validity of the asymptotic responses determined in the previous sections, the pitchfork bifurcation separating the pre- and post-buckling solutions is here investigated. Such bifurcation corresponds to the static bifurcation of system equilibria defined by relation (3) when the analysis is extended to the dynamic nonlinear regime. Thus, as before, its occurrence is induced by the vanishing of the linear mechanical stiffness. The study is performed by referring to the dynamical system around $\mathbf{e_1}$ equilibrium (4), when the linear frequency is scaled according to $\omega^2 = \epsilon\hat{\omega}^2$ (with the hat thereafter skipped),

in addition to the observations on the scaling of parameters and variables made in Section 3. It can be deduced that the bifurcation under analysis is associated with a Jordan block of the Jacobian matrix leading to a double-zero eigenvalue. As shown in the literature, the double-zero bifurcation has to be analysed by means of fractional power series expansions [34, 35]. The asymptotic procedure is presented in Appendix D, and calls for the introduction of three time scales, i.e., $T_0 = t$, $T_1 = \epsilon^{1/2}t$, $T_2 = \epsilon t$, and for the scaling of the mechanical harmonic excitation to the generating order due to the nonresonant region under analysis, according to the following perturbation scheme:

- Order ϵ **Mechanical equation:** external excitation (complementary and particular solution)
- Order $\epsilon^{3/2}$ **Mechanical equation:** correction
  Thermal equations: mechanical coupling terms (a_{24}, a_{33})
- Order ϵ^2 **Mechanical equation:** linear stiffness, cubic term, damping, thermal coupling terms (a_{15}, a_{16})

The resulting real amplitude modulation equation for the mechanical displacement, which is an order-2 differential equation, is

$$\ddot{A} = c_1 A + c_3 A^3 \tag{16}$$

where c_1 and c_3 coefficients are defined in Appendix D. The fixed points of Eq. (16) are obtained by setting $A = \text{cost}$, and read

$$\boldsymbol{A_e} = \{0, \sqrt{\frac{\omega^2(p) - c_{11}f^2}{c_3}}, -\sqrt{\frac{\omega^2(p) - c_{11}f^2}{c_3}}\} \tag{17}$$

where $c_{11} = \frac{2a_{16}a_{24}}{4a_{22}^2\Omega^2+4\Omega^4} - \frac{3a_{14}}{2\Omega^4}$. In (17), it is worth noting the dependence of the fixed points on both mechanical excitations, i.e. precompression p and harmonic forcing amplitude f, which are chosen as control parameters to investigate the variation of the fixed points.

Figure 8 shows the fixed points evolution in the (p, f, A) space, and highlights the effect of the harmonic forcing amplitude on the behavior of the nontrivial fixed points, which arise for higher and higher p values as the forcing amplitude increases. In particular, the AME fixed points are seen to coincide with the static equilibria $\mathbf{e_{1,2,3}}$ of the system (red curves) when the unforced system is considered. In fact, recalling the expression of ω^2 ((5)) and that of c_3 coefficient, it is straightforward to reduce Eqs. (17) to Eqs.(2) when $f = 0$. The pitchfork bifurcation is detected by the fixed point intersection, i.e., double-zero bifurcation occurs when $A_{e_2,e_3} = 0$, corresponding to

$$f = \frac{\omega(p)}{\sqrt{c_{11}}} \tag{18}$$

The pitchfork bifurcation threshold in the (p, f) plane is reported in Fig.9(a) with dashed lines. In particular, the asymptotic relation (18) (red dashed curve) is compared with numerical outcomes obtained through continuation technique (black dashed curve). The saddle-node bifurcation loci deriving from the previous

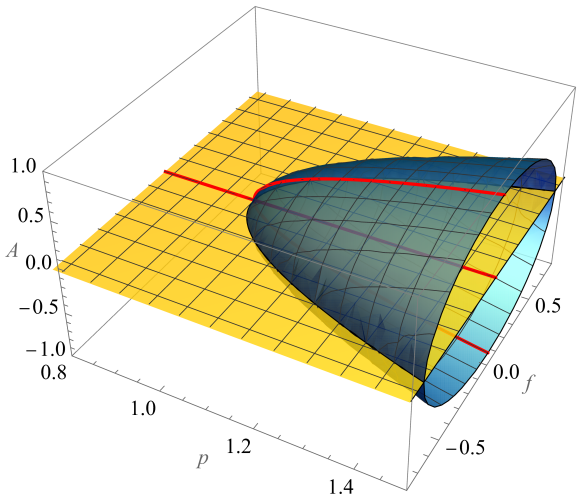

Fig. 8 For $\Omega = 1$ and $T_\infty = 0$, fixed points $\boldsymbol{A_e}$ of AME (16) in the (p, f, A) space. (Color figure online)

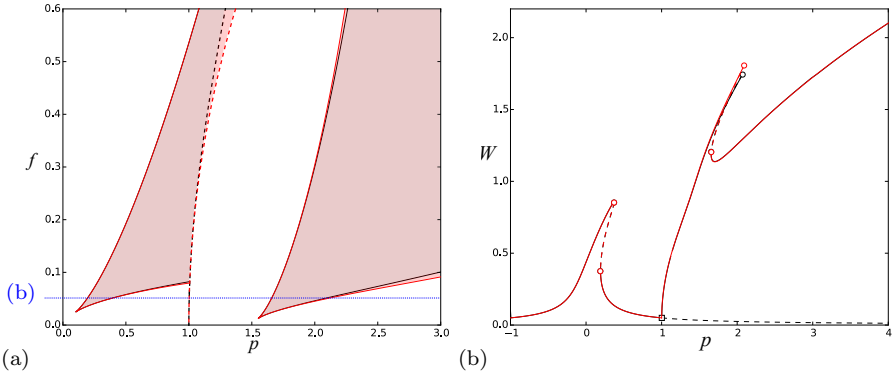

Fig. 9 For $\Omega = 1$ and $T_\infty = 0$, stability chart in the (p, f) plane (a); Bifurcation diagram of the maximum displacement W for $f = 0.05$ (b). Black lines: numerical ODEs integration; red lines: asymptotic results. Saddle-node bifurcation: solid lines (a)/circle (b); Pitchfork bifurcation: dashed lines (a)/square (b). Red regions: asymptotic bistability; overlapped gray/red regions: numerical/asymptotic bistability. (Color figure online)

analyses at pre- and post-buckling resonances (represented by circles in Figs. 3, 5 and 9(b)) are also reported in Fig. 9(a) by solid lines.

Indeed, the figure represents a chart characterizing the overall behavior of the system in terms of stability of all detected 1-period solutions, thus including and summarizing the results presented in the previous sections. The saddle-node bifurcations identify bistability regions (coloured regions) characterized by the concurrent presence of resonant and nonresonant responses, which exist around pre- and

post-buckling resonances. The pitchfork bifurcation ensuing from the asymptotic treatment herein accomplished separates the ranges of applicability of the results obtained in the pre-buckling and post-buckling regimes. For easier reading of the chart, Figure 9(b) shows the bifurcation diagram of the maximum value of the mechanical displacement W, for $f = 0.05$ and in a range of precompression values such to include both pre- and post-buckling resonance regions.

With a view to validating the analytical results, the chart confirms the excellent ability of the presented analyses to reproduce the overall response of the system, not only in terms of amplitude of the mechanical and thermal responses, but also as regards their existence and stability, marked by the various identified local bifurcations, even for moderately high values of the excitation parameters. In fact, the analytical red curves and regions in Fig. 9(a) are almost completely indistinguishable from the black curves (and ensuing gray regions) obtained via continuation of the numerical outcomes from ODEs (1), just with slight discrepancies when moving away from the resonance conditions or for high values of the forcing amplitude.

6 Conclusions

The weakly nonlinear dynamics of a thermomechanical plate has been investigated by means of asymptotic approaches aimed at understanding and describing the main dynamical phenomena which underly the rich multistable scenario characterizing the strong nonlinear behavior. For low values of the mechanical forcing excitation, three main dynamical phenomena have been investigated, namely the responses at primary resonance around pre- and post-buckling equilibria, and a double-zero bifurcation marking the dynamical buckling of the plate.

The different features of the equation systems governing the dynamics in pre- and post-buckling regimes has called for the development of specific asymptotic procedures. Moreover, the multiphysics context characterized by the contemporary presence of thermal (slow) and mechanical (fast) dynamics has required a careful evaluation in the scaling of variables as well as of coupling terms into the mechanical and thermal equations. The analytical outcomes of the investigations around the two primary resonances reveal that the mechanical amplitude is governed by formally identical equations in pre-buckling and post-buckling conditions, of course with a different expression of the coefficients. Differently, the reconstructed mechanical and thermal solutions in post-buckling regime are characterized by a much richer content of superharmonic contributions than in the pre-buckling case, due to the higher asymptotic order which has been necessary to achieve in order to account for all the attain and coupling terms exhibited by the model.

To analytically determine the bifurcation equation describing the dynamical buckling, a fractional-order multiple scale approach has been applied to the system with vanishing linear stiffness. The equilibrium analysis of the ensuing order-2 differential equation describing the dynamics of the real mechanical amplitude has proved to be efficient in furnishing the frequency-forcing amplitude relation describing the boundary between pre- and post-buckling behaviors.

All asymptotic procedures have demonstrated their ability in grasping the actual dynamics of the thermomechanical model obtained by numerical simulations,

overall framing the relevant results within a consistent and comprehensive interpretative scenario. Reliability of the analytical results has been verified in terms of existence and stability of the detected periodic responses, as well as in terms of portraits of the mechanical and thermal solutions in the phase plane. It is worth underlining that the proposed procedures account for the possible contemporary variation of both mechanical excitations, represented by in-plane precompression and transversal harmonic forcing, and thermal boundary condition accounting for free heat exchange between plate and environment. As a consequence, the obtained analytical relations represent a manageable and versatile tool for parametric analysis and design of plate dynamics in a full thermomechanical environment. Of course, considering different thermal boundary conditions would lead to a different set of equations of motion, as illustrated in [22, 24], which would require a different organization of all asymptotic procedures.

Appendix A Material properties and equation coefficients

The dynamical behavior of the thermomechanical model is investigated by considering an epoxy/carbon fibre composite plate of dimensions $a = b = 1$ m and $h = 0.01$ m. The material's elastic and thermal properties, which are assumed to be independent of the temperature, are taken from [36], and read:

$$\begin{aligned} &Y_1 = 1.72 \cdot 10^{11} \frac{N}{m^2},\ \nu_{12} = 0.25,\ \rho = 1940 \frac{kg}{m^3},\ \lambda_{11} = 36.42 \frac{W}{m \cdot K}, \\ &\alpha_1 = 0.57 \cdot 10^{-6} \frac{1}{K},\ Y_2 = 6.91 \cdot 10^{9} \frac{N}{m^2},\ G_{12} = 3.45 \cdot 10^{9} \frac{N}{m^2}, \\ &\lambda_{22} = 0.96 \frac{W}{m \cdot K},\ \alpha_2 = 35.6 \cdot 10^{-6} \frac{1}{K},\ c_v = 400 \frac{J}{kg \cdot K}, \\ &\delta = 330 \frac{N \cdot s}{m^3},\ H = 100 \frac{W}{m^2 \cdot K} \end{aligned} \tag{19}$$

where Y_1, Y_2, G_{12} are longitudinal modulus of rigidity in x and y direction and shear modulus, respectively; ν_{12} is the Poisson's ratio; ρ and δ are mass density and damping coefficient; $\lambda_{11}, \lambda_{22}, \lambda_{33}$ are the thermal conductivities along the x, y and z directions; α_1, α_2 are the thermal expansions along x and y directions; c_v is the specific heat at constant strain, and H is the boundary conductance. The subsequent value of the mechanical natural frequency is $286.67 Hz$. After nondimensionalization, the numerical coefficients of Eqs. (1) are:

$$\begin{aligned} &a_{12} = 0.0593,\ a_{14} = 0.6859,\ a_{15} = -0.2729,\ a_{16} = -0.9036, \\ &a_{22} = 7.81 \cdot 10^{-5},\ a_{23} = -1.2391,\ a_{24} = 1.08 \cdot 10^{-4}, \\ &a_{32} = 6.06 \cdot 10^{-4},\ a_{33} = 0.001195 \end{aligned} \tag{20}$$

Appendix B Multiple Scale analysis of the pre-buckling equilibrium

To develop the asymptotic procedure to the system (4), three time scales are introduced, i.e., $T_0 = t,\ T_1 = \epsilon t,\ T_2 = \epsilon^2 t$, and, consistently, the time derivatives are expressed as

$$\begin{aligned} &d/dt = D_0 + \epsilon D_1 + \epsilon^2 D_2 \\ &d^2/dt^2 = D_0^2 + 2\epsilon D_0 D_1 + \epsilon^2 D_1^2 + 2\epsilon^2 D_0 D_2 \end{aligned} \tag{21}$$

where $D_i = \partial / \partial T_i$. Due to the presence of only cubic nonlinear term in the mechanical equation, and in order to account for the different time evolution of the mechanical variable with respect to the thermal ones, variables are scaled as follows:

$$\tilde{W} = \epsilon^{1/2}\, \hat{W}, \qquad \tilde{T}_{R0} = \epsilon^{3/2}\, \hat{T}_{R0}, \qquad \tilde{T}_{R1} = \epsilon^{3/2}\, \hat{T}_{R1} \tag{22}$$

so that their expression as perturbation of the reference equilibrium reads:

$$\begin{aligned} &\tilde{W}(t) = \epsilon^{1/2} W_0(T_0, T_1, T_2) + \epsilon^{3/2} W_1(T_0, T_1, T_2) + \epsilon^{5/2} W_2(T_0, T_1, T_2) \\ &\tilde{T}_{R0}(t) = \epsilon^{3/2} T0_0(T_0, T_1, T_2) + \epsilon^{5/2} T0_1(T_0, T_1, T_2) + \epsilon^{7/2} T0_2(T_0, T_1, T_2) \\ &\tilde{T}_{R1}(t) = \epsilon^{3/2} T1_0(T_0, T_1, T_2) + \epsilon^{5/2} T1_1(T_0, T_1, T_2) + \epsilon^{7/2} T1_2(T_0, T_1, T_2) \end{aligned} \tag{23}$$

Parameter scaling is performed by assuming small damping and small transversal excitation, while coupling terms are scaled to properly account for the different time scale at which thermal variables evolve with respect to the mechanical one:

$$a_{12} = \epsilon\, \hat{a}_{12}, \quad f = \epsilon^{3/2}\, \hat{f}, \quad a_{15} = \epsilon\, \hat{a}_{15}, \quad a_{16} = \epsilon^{1/2}\, \hat{a}_{16}, \quad a_{24} = \epsilon^{1/2}\, \hat{a}_{24}, \quad a_{33} = \epsilon\, \hat{a}_{33} \tag{24}$$

To study the response around primary resonance, detuning parameter σ is introduced:

$$\omega^2 = \Omega^2 + \epsilon\, \sigma \tag{25}$$

Once scaled by $\epsilon^{-1/2}$, the resulting perturbation equations at each order read:

- Order ϵ $$D_0^2 W_0 + \Omega^2 W_0 = 0 \tag{26}$$
- Order ϵ^2 $$\begin{aligned} &D_0^2 W_1 + \Omega^2 W_1 = -a_{12} D_0 W_0 - a_{14} W_0^3 - 2 D_0 D_1 W_0 - \sigma W_0 + f\cos(\Omega T_0) \\ &D_0 \mathrm{T0}_0 + a_{22} \mathrm{T0}_0 = -a_{24} W_0 D_0 W_0 \\ &D_0 \mathrm{T1}_0 + a_{32} \mathrm{T1}_0 = -a_{33} D_0 W_0 \end{aligned} \tag{27}$$
- Order ϵ^3 $$\begin{aligned} &D_0^2 W_2 + W_2 \Omega^2 = -a_{12} D_0 W_1 - a_{12} D_1 W_0 - 3 a_{14} W_1 W_0^2 - a_{15} \mathrm{T1}_0 \\ &- a_{16} \mathrm{T0}_0 W_0 - 2 D_0 D_1 W_1 - D_1^2 W_0 - 2 D_0 D_2 W_0 - \sigma W_1 \\ &D_0 \mathrm{T0}_1 + a_{22} \mathrm{T0}_1 = -a_{24} W_0 D_0 W_1 - a_{24} W_0 D_1 W_0 - a_{24} W_1 D_0 W_0 - D_1 \mathrm{T0}_0 \\ &D_0 \mathrm{T1}_1 + a_{32} \mathrm{T1}_1 = -a_{33} D_0 W_1 - a_{33} D_1 W_0 - D_1 \mathrm{T1}_0 \end{aligned} \tag{28}$$

At first order, the solution of the mechanical equation (26) reads

$$W_0 = A(T_1, T_2) \mathrm{e}^{i\Omega T_0} + c.c. \tag{29}$$

with $A(T_1, T_2)$ undetermined function of the slow time scales and *c.c.* complex conjugate terms (the overbar will denote the complex conjugate and i is the imaginary unit). Substituting W_0 in the first equation of (27), and imposing the solvability condition implies

$$D_1 A = \frac{i\left(-f + 2(\sigma + i a_{12}\Omega)A + 6 a_{14} A^2 \bar{A}\right)}{4\Omega} \tag{30}$$

The particular solutions at order ϵ^2 are

$$\begin{aligned} W_1 &= \frac{a_{14} A^3 \mathrm{e}^{3i\Omega T_0}}{8\Omega^2} + c.c. \\ \mathrm{T0}_0 &= \frac{a_{24}\Omega A^2 \mathrm{e}^{2i\Omega T_0}}{i a_{22} - 2\Omega} + c.c. \\ \mathrm{T1}_0 &= \frac{a_{33}\Omega A \mathrm{e}^{i\Omega T_0}}{i a_{32} - \Omega} + c.c. \end{aligned} \tag{31}$$

In view of Eqs. (29)-(31), the solvability condition of the mechanical problem at the third order (28) yields

$$D_2 A = c_{1r} + i c_{1i} + (c_{2r} + i c_{2i}) A + i c_{3i} A^2 - 2 i c_{3i} A \bar{A} + (c_{4r} + i c_{4i}) A^2 \bar{A} + i c_{5i} A^3 \bar{A}^2 \tag{32}$$

where

$$\begin{aligned} &c_{1r} = \frac{a_{12} f}{16\Omega^2},\ c_{1i} = \frac{f\sigma}{16\Omega^3},\ c_{2r} = \frac{a_{15} a_{32} a_{33}}{2\left(a_{32}^2 + \Omega^2\right)},\ c_{2i} = -\frac{a_{12}^2}{8\Omega} - \frac{a_{15} a_{33}\Omega}{2\left(a_{32}^2 + \Omega^2\right)} - \frac{\sigma^2}{8\Omega^3}, \\ &c_{3i} = -\frac{3 a_{14} f}{16\Omega^3},\ c_{4r} = \frac{3 a_{12} a_{14}}{4\Omega^2} + \frac{a_{16} a_{22} a_{24}}{2\left(a_{22}^2 + 4\Omega^2\right)},\ c_{4i} = -\frac{3 a_{14}\sigma}{4\Omega^3} - \frac{a_{16} a_{24}\Omega}{a_{22}^2 + 4\Omega^2},\ c_{5i} = -\frac{15 a_{14}^2}{16\Omega^3} \end{aligned} \tag{33}$$

According to the usual reconstitution procedure [37], the amplitude derivatives with respect to time t are obtained from (21)

$$\dot{A} = \epsilon D_1 A + \epsilon^2 D_2 A \tag{34}$$

The ϵ parameter is completely reabsorbed through a backward rescaling, and recalling Eqs. (30) and (32), the complex amplitude modulation equation for the mechanical variable results

$$\dot{A} = c_{1r} + i c_{11i} + (c_{21r} + i c_{21i}) A + i c_{3i} A^2 - 2 i c_{3i} A \bar{A} + (c_{4r} + i c_{41i}) A^2 \bar{A} + i c_{5i} A^3 \bar{A}^2 \tag{35}$$

where

$$c_{11i} = -\frac{f}{4\Omega} + c_{1i},\ c_{21r} = c_{2r} - \frac{a_{12}}{2},\ c_{21i} = c_{2i} + \frac{\sigma}{2\Omega},\ c_{41i} = \frac{3 a_{14}}{2\Omega} + c_{4i} \tag{36}$$

The complex-valued modulation equation for the mechanical amplitude A can be conveniently expressed in polar form applying the following transformation

$$A = \frac{1}{2}a(t)\mathrm{e}^{i\theta(t)},\ \bar{A} = \frac{1}{2}a(t)\mathrm{e}^{-i\theta(t)} \tag{37}$$

Separating real and imaginary parts leads

$$\begin{aligned}\dot{a} &= 2(c_{11i}\sin\theta + c_{1r}\cos\theta) + c_{21r}a - \frac{3c_{3i}a^2\sin\theta}{2} + \frac{c_{4r}a^3}{4} \\ a\dot{\theta} &= 2(c_{11i}\cos\theta - c_{1r}\sin\theta) + c_{21i}a - \frac{c_{3i}a^2\cos\theta}{2} + \frac{c_{41i}a^3}{4} + \frac{c_{5i}a^5}{16}\end{aligned} \tag{38}$$

where the time dependence of a and θ has been omitted for the sake of readability. Finally, the system asymptotic solutions can be reconstructed at second order by recalling equations (29) and (31). Moreover, remembering that $W(t) = W_{e_1} + \tilde{W}$, $T_{R0}(t) = T_{R0e_1} + \tilde{T}_{R0}$, $T_{R1}(t) = T_{R1e_1} + \tilde{T}_{R1}$, mechanical and thermal solutions can be expressed in trigonometric form as

$$W(t) = a\cos\psi + c_6\ a^3\cos(3\psi) \tag{39}$$

$$T_{R0}(t) = T_{R0e_1} + c_7\ a^2\cos(2\psi) + c_8\ a^2\sin(2\psi) \tag{40}$$

$$T_{R1}(t) = c_9\ a\cos\psi + c_{10}\ \sin\psi \tag{41}$$

where $\psi = \Omega t + \theta$ and

$$c_6 = \frac{a_{14}}{32\Omega^2},\ c_7 = -\frac{a_{24}\Omega^2}{a_{22}^2 + 4\Omega^2},\ c_8 = \frac{a_{22}a_{24}\Omega}{2\left(a_{22}^2 + 4\Omega^2\right)},\ c_9 = -\frac{a_{33}\Omega^2}{a_{32}^2 + \Omega^2},\ c_{10} = \frac{a_{32}a_{33}\Omega}{a_{32}^2 + \Omega^2}$$

Appendix C Multiple Scale analysis of the post-buckling equilibrium

Due to the presence of quadratic and cubic nonlinear terms in the mechanical equation (10), five time scales are introduced, i.e., $T_0 = t,\ T_1 = \epsilon t,\ T_2 = \epsilon^2 t,\ T_3 = \epsilon^3 t,\ T_4 = \epsilon^4 t$, so that time derivatives are expressed as

$$\begin{aligned}&d/dt = D_0 + \epsilon D_1 + \epsilon^2 D_2 + \epsilon^3 D_3 + \epsilon^4 D_4 \\ &d^2/dt^2 = D_0^2 + 2\epsilon D_0 D_1 + \epsilon^2(D_1^2 + 2D_0 D_2) + 2\epsilon^3(D_1 D_2 + D_0 D_3) \\ &+ \epsilon^4(D_2^2 + 2D_1 D_3 + 2D_0 D_4)\end{aligned} \tag{42}$$

where $D_i = \partial/\partial T_i$. To account for the different time evolution of the mechanical variable with respect to the thermal ones, variables are scaled as follows:

$$\tilde{W} = \epsilon\,\hat{W}, \qquad \tilde{T}_{R0} = \epsilon^2\,\hat{T}_{R0}, \qquad \tilde{T}_{R1} = \epsilon^2\,\hat{T}_{R1} \tag{43}$$

so that their expression as perturbation of the reference equilibrium reads:

$$\begin{aligned}&\tilde{W}(t) = \epsilon W_0(T_0,T_1,T_2,T_3,T_4) + \epsilon^2 W_1(T_0,T_1,T_2,T_3,T_4) + \epsilon^3 W_2(T_0,T_1,T_2,T_3,T_4) \\ &+ \epsilon^4 W_3(T_0,T_1,T_2,T_3,T_4) + \epsilon^5 W_4(T_0,T_1,T_2,T_3,T_4) \\ &\tilde{T}_{R0}(t) = \epsilon^2 T0_0(T_0,T_1,T_2,T_3,T_4) + \epsilon^3 T0_1(T_0,T_1,T_2,T_3,T_4) + \epsilon^4 T0_2(T_0,T_1,T_2,T_3,T_4) \\ &+ \epsilon^5 T0_3(T_0,T_1,T_2,T_3,T_4) + \epsilon^6 T0_4(T_0,T_1,T_2,T_3,T_4) \\ &\tilde{T}_{R1}(t) = \epsilon^2 T1_0(T_0,T_1,T_2,T_3,T_4) + \epsilon^3 T1_1(T_0,T_1,T_2,T_3,T_4) + \epsilon^4 T1_2(T_0,T_1,T_2,T_3,T_4) \\ &+ \epsilon^5 T1_3(T_0,T_1,T_2,T_3,T_4) + \epsilon^6 T1_4(T_0,T_1,T_2,T_3,T_4)\end{aligned} \tag{44}$$

As for the pre-buckling resonance analysis, parameter scaling is performed by assuming small damping and small transversal excitation, while coupling terms are scaled to properly account for the different time scale at which thermal variables evolve with respect to the mechanical

one. Due to the increased number of time scales considered and to the different contributions into mechanical and membrane thermal equations, parameter scaling is adjusted as follows:

$$a_{12} = \epsilon^2\,\hat{a}_{12}, \quad a_{15} = \epsilon^2\,\hat{a}_{15}, \quad a_{16} = \epsilon^2\,\hat{a}_{16}, \quad f = \epsilon^3\,\hat{f}, \quad a_{24} = \epsilon\,\hat{a}_{24}, \quad a_{33} = \epsilon\,\hat{a}_{33} \tag{45}$$

To study the response around primary resonance, detuning parameter σ is introduced:

$$\omega^2 = \Omega^2 + \epsilon^2\,\sigma \tag{46}$$

while ω is derived from the square root of (46) through series expansion to the first order around $\sigma = 0$: $\omega = \Omega + \epsilon^2\sigma/(2\Omega) + \mathcal{O}(\sigma^2)$.

The resulting perturbation equations at each order read:

- Order ϵ
$$D_0^2 W_0 + \Omega^2 W_0 = 0 \tag{47}$$

- Order ϵ^2
$$\begin{aligned} &D_0^2 W_1 + \Omega^2 W_1 = -2D_0D_1W_0 - \frac{3\Omega W_0^2}{2a_{141}} \\ &D_0\mathrm{T0}_0 + a_{22}\mathrm{T0}_0 = -a_{141}a_{24}\Omega D_0 W_0 \\ &D_0\mathrm{T1}_0 + a_{32}\mathrm{T1}_0 = -_{33}D_0W_0 \end{aligned} \tag{48}$$

- Order ϵ^3
$$\begin{aligned} &D_0^2 W_2 + \Omega^2 W_2 = -a_{12}D_0W_0 - \frac{3\Omega W_1 W_0}{a_{141}} - a_{14}W_0^3 \\ &- 2D_0D_1W_1 - D_1^2W_0 - 2D_0D_2W_0 - \sigma W_0 + f\cos(\Omega T_0) \\ &D_0\mathrm{T0}_1 + a_{22}\mathrm{T0}_1 = -a_{141}a_{24}\Omega D_0W_1 - a_{141}a_{24}\Omega D_1W_0 \\ &- a_{24}W_0D_0W_0 - D_1\mathrm{T0}_0 \\ &D_0\mathrm{T1}_1 + a_{32}\mathrm{T1}_1 = -a_{33}D_0W_1 - a_{33}D_1W_0 - D_1\mathrm{T1}_0 \end{aligned} \tag{49}$$

- Order ϵ^4
$$\begin{aligned} &D_0^2 W_3 + \Omega^2 W_3 = -a_{12}D_0W_1 - a_{12}D_1W_0 - 3a_{14}W_1W_0^2 - a_{141}a_{16}\mathrm{T0}_0\Omega \\ &- \frac{3\sigma W_0^2}{4a_{141}\Omega} - \frac{3W_2W_0\Omega}{a_{141}} - \frac{3W_1^2\Omega}{2a_{141}} - a_{15}\mathrm{T1}_0 - 2D_0D_1W_2 - D_1^2W_1 \\ &- 2D_0D_2W_1 - 2D_1D_2W_0 - 2D_0D_3W_0 - \sigma W_1 \\ &D_0\mathrm{T0}_2 + a_{22}\mathrm{T0}_2 = -\frac{a_{141}a_{24}\sigma D_0W_0}{2\Omega} - a_{141}a_{24}\Omega D_0W_2 - a_{141}a_{24}\Omega D_1W_1 \\ &- a_{141}a_{24}\Omega D_2W_0 - a_{24}W_0D_0W_1 - a_{24}W_0D_1W_0 - a_{24}W_1D_0W_0 \\ &- D_1\mathrm{T0}_1 - D_2\mathrm{T0}_0 \\ &D_0\mathrm{T1}_2 + a_{32}\mathrm{T1}_2 = -a_{33}D_0W_2 - a_{33}D_1W_1 - a_{33}D_2W_0 - D_1\mathrm{T1}_1 - D_2\mathrm{T1}_0 \end{aligned} \tag{50}$$

- Order ϵ^5
$$\begin{aligned} &D_0^2 W_4 + \Omega^2 W_4 = -a_{12}D_0W_2 - a_{12}D_1W_1 - a_{12}D_2W_0 - 3a_{14}W_2W_0^2 \\ &- 3a_{14}W_1^2W_0 - a_{141}a_{16}\mathrm{T0}_1\Omega - \frac{3\sigma W_1W_0}{2a_{141}\Omega} - \frac{3W_3W_0\Omega}{a_{141}} - \frac{3W_1W_2\Omega}{a_{141}} \\ &- a_{15}\mathrm{T1}_1 - a_{16}\mathrm{T0}_0W_0 - 2D_0D_1W_3 - D_1^2W_2 - 2D_0D_2W_2 - 2D_1D_2W_1 \\ &- D_2^2W_0 - 2D_0D_3W_1 - 2D_1D_3W_0 - 2D_0D_4W_0 - \sigma W_2 \\ &D_0\mathrm{T0}_3 + a_{22}\mathrm{T0}_3 = -\frac{a_{141}a_{24}\sigma D_0W_1}{2\Omega} - \frac{a_{141}a_{24}\sigma D_1W_0}{2\Omega} - a_{141}a_{24}\Omega D_0W_3 \\ &- a_{141}a_{24}\Omega D_1W_2 - a_{141}a_{24}\Omega D_2W_1 - a_{141}a_{24}\Omega D_3W_0 - a_{24}W_0D_0W_2 \\ &- a_{24}W_0D_1W_1 - a_{24}W_0D_2W_0 - a_{24}W_1D_0W_1 - a_{24}W_1D_1W_0 \\ &- a_{24}W_2D_0W_0 - D_1\mathrm{T0}_2 - D_2\mathrm{T0}_1 - D_3\mathrm{T0}_0 \\ &D_0\mathrm{T1}_3 + a_{32}\mathrm{T1}_3 = -a_{33}D_0W_3 - a_{33}D_1W_2 - a_{33}D_2W_1 - a_{33}D_3W_0 \\ &- D_1\mathrm{T1}_2 - D_2\mathrm{T1}_1 - D_3\mathrm{T1}_0 \end{aligned} \tag{51}$$

At first order, the solution of the mechanical equation (47) reads

$$W_0 = A(T_1, T_2, T_3, T_4)\mathrm{e}^{i\Omega T_0} + c.c. \tag{52}$$

with $A(T_1, T_2, T_3, T_4)$ undetermined function of the slow time scales. Substituting W_0 in the first equation of (48), and imposing the solvability condition implies

$$D_1 A = 0 \tag{53}$$

The particular solutions at order ϵ^2 are

$$\begin{aligned} W_1 &= -\frac{3A\bar{A}}{a_{141}\Omega} + \frac{A^2 \mathrm{e}^{2i\Omega T_0}}{2a_{141}\Omega} + c.c. \\ T0_0 &= \frac{a_{141}a_{24}\Omega^2 A \mathrm{e}^{i\Omega T_0}}{ia_{22}-\Omega} + c.c. \\ T1_0 &= \frac{a_{33}\Omega A e^{i\Omega T_0}}{ia_{32}-\Omega} + c.c. \end{aligned} \tag{54}$$

Moving to the third order, equations (52)-(54) are substituted into equations (49); removing secular terms into the mechanical equation leads to

$$D_2 A = \frac{i\left(-f + 2(\sigma + ia_{12}\Omega)A - 24a_{14}A^2\bar{A}\right)}{4\Omega} \tag{55}$$

Mechanical and thermal solutions at third order result

$$\begin{aligned} W_2 &= \left(\frac{a_{14}}{8\Omega^2} + \frac{3}{16a_{141}^2\Omega^2}\right) A^3 \mathrm{e}^{3i\Omega T_0} + c.c. \\ T0_1 &= \frac{2a_{24}\Omega}{+ia_{22}-2\Omega} A^2 \mathrm{e}^{2i\Omega T_0} + c.c. \\ T1_1 &= \frac{a_{33}}{a_{141}(ia_{32}-2\Omega)} A^2 \mathrm{e}^{2i\Omega T_0} + c.c. \end{aligned} \tag{56}$$

At fourth order, after substitution of solvability conditions and particular solutions at the previous orders, eliminating secular terms implies

$$D_3 A = \frac{i}{2}\left(\frac{a_{141}^2 a_{16}a_{24}\Omega^2}{ia_{22}-\Omega} + \frac{a_{15}a_{33}}{ia_{32}-\Omega}\right) A \tag{57}$$

Particular solutions at fourth order read

$$\begin{aligned} W_3 &= \frac{3\sigma A\bar{A}}{4a_{141}\Omega^3} + \frac{3\left(20a_{14}a_{141}^2 - 19\right)}{8a_{141}^3\Omega^3} A^2\bar{A}^2 \\ &+ \left(\frac{fA}{3a_{141}\Omega^3} + \frac{7\left(14a_{14}a_{141}^2 - 3\right)}{16a_{141}^3\Omega^3} A^3\bar{A} - \frac{3\sigma + 4ia_{12}\Omega}{12a_{141}\Omega^3} A^2\right) \mathrm{e}^{2i\Omega T_0} \\ &+ \frac{2a_{14}a_{141}^2 + 1}{16a_{141}^3\Omega^3} A^4 \mathrm{e}^{4i\Omega T_0} + c.c. \\ T0_2 &= \left(\frac{ia_{141}a_{22}a_{24}f}{4(a_{22}+i\Omega)^2} + \frac{a_{141}a_{24}(a_{12}a_{22}\Omega - 2ia_{22}\sigma + \sigma\Omega)A}{2(a_{22}+i\Omega)^2}\right. \\ &\left. + \frac{ia_{24}\left(a_{22}\left(12a_{14}a_{141}^2 + 5\right) + 5i\Omega\right) A^2\bar{A}}{2a_{141}(a_{22}+i\Omega)^2}\right) \mathrm{e}^{i\Omega T_0} - \frac{3ia_{24}\left(2a_{14}a_{141}^2 + 11\right) A^3 \mathrm{e}^{3i\Omega T_0}}{16a_{141}(a_{22}+3i\Omega)} + c.c. \\ T1_2 &= \left(\frac{ia_{32}a_{33}f}{4\Omega(a_{32}+i\Omega)^2} + \frac{a_{32}a_{33}(a_{12}\Omega - i\sigma)A}{2\Omega(a_{32}+i\Omega)^2} + \frac{6ia_{14}a_{32}a_{33}A^2\bar{A}}{\Omega(a_{32}+i\Omega)^2}\right) \mathrm{e}^{i\Omega T_0} \\ &- \frac{3ia_{33}\left(2a_{14}a_{141}^2 + 3\right) A^3 \mathrm{e}^{3i\Omega T_0}}{16a_{141}^2\Omega(a_{32}+3i\Omega)} + c.c. \end{aligned} \tag{58}$$

Finally, at fifth order, solvability condition for the mechanical equation of (51) provides

$$\begin{aligned} D_4 A &= \frac{f(a_{12}\Omega + i\sigma)}{16\Omega^3} - \frac{i\left(a_{12}^2\Omega^2 + \sigma^2\right) A}{8\Omega^3} + \frac{3ia_{14}fA^2}{4\Omega^3} - \frac{ia_{14}fA\bar{A}}{2\Omega^3} \\ &+ \frac{a_{14}(-2a_{12}\Omega + 3i\sigma)A^2\bar{A}}{\Omega^3} - \frac{27ia_{14}^2A^3\bar{A}^2}{\Omega^3} \end{aligned} \tag{59}$$

According to the usual reconstitution procedure [37], the amplitude derivatives with respect to time t are obtained from (21)

$$\dot{A} = \epsilon D_1 A + \epsilon^2 D_2 A + \epsilon^3 D_3 A + \epsilon^4 D_4 A \tag{60}$$

The ϵ parameter is completely reabsorbed through a backward rescaling, and recalling Eqs. (53), (55), (57), (59), the complex amplitude modulation equation for the mechanical variable results

$$\dot{A} = c_{1r} + ic_{1i} + (c_{2r} + ic_{2i})A + ic_{3i}A\bar{A} - \frac{3}{2}ic_{3i}A^2 + (c_{4r} + ic_{4i})A^2\bar{A} + ic_{5i}A^3\bar{A}^2 \tag{61}$$

where

$$\begin{aligned}
&c_{1r} = \frac{a_{12}f}{16\Omega^2},\ c_{1i} = \frac{f\left(\sigma - 4\Omega^2\right)}{16\Omega^3},\ c_{2r} = -\frac{a_{12}}{2} + \frac{a_{16}a_{22}a_{24}\Omega^2}{4a_{14}\left(a_{22}^2 + \Omega^2\right)} + \frac{a_{15}a_{32}a_{33}}{2\left(a_{32}^2 + \Omega^2\right)},\\
&c_{2i} = -\frac{a_{12}^2\Omega^2 + \sigma^2 - 4\sigma\Omega^2}{8\Omega^3} - \frac{a_{16}a_{24}\Omega^3}{4a_{14}\left(a_{22}^2 + \Omega^2\right)} - \frac{a_{15}a_{33}\Omega}{2\left(a_{32}^2 + \Omega^2\right)},\ c_{3i} = -\frac{a_{14}f}{2\Omega^3},\\
&c_{4r} = -\frac{2a_{12}a_{14}}{\Omega^2},\ c_{4i} = \frac{3a_{14}\left(\sigma - 2\Omega^2\right)}{\Omega^3},\ c_{5i} = -\frac{27a_{14}^2}{\Omega^3}
\end{aligned} \tag{62}$$

The complex-valued modulation equation for the mechanical amplitude A can be conveniently expressed in polar form applying the following transformation

$$A = \frac{1}{2}a(t)\mathrm{e}^{i\theta(t)},\ \bar{A} = \frac{1}{2}a(t)\mathrm{e}^{-i\theta(t)} \tag{63}$$

Separating real and imaginary parts leads

$$\dot{a} = +2(c_{1i}\sin\theta + c_{1r}\cos\theta) + c_{2r}a + \frac{5c_{3i}a^2\sin\theta}{4} + \frac{c_{4r}a^3}{4} \tag{64}$$

$$a\dot{\theta} = 2(c_{1i}\cos\theta - c_{1r}\sin\theta) + c_{2i}a - \frac{c_{3i}a^2\cos\theta}{4} + \frac{c_{4i}a^3}{4} + \frac{c_{5i}a(t)^5}{16} \tag{65}$$

where the time dependence of a and θ has been omitted for the sake of readability. Finally, the system asymptotic solutions can be reconstructed at fourth order by recalling equations (52), (54), (56), (58). Moreover, remembering that $W(t) = W_{e_2} + \tilde{W}$, $T_{R0}(t) = T_{R0e_2} + \tilde{T}_{R0}$, $T_{R1}(t) = T_{R1e_2} + \tilde{T}_{R1}$, mechanical and thermal solutions can be expressed in trigonometric form as

$$\begin{aligned}
W(t) &= W_{e_2} - 3c_6a^2 - 27c_7a^4 + a\cos\psi + c_8a\cos(2\psi - \theta) + (c_6a^2 + 14c_7a^4)\cos(2\psi)\\
&+ c_9a^2\sin(2\psi) + c_{10}a^3\cos(3\psi) + c_7a^4\cos(4\psi)
\end{aligned} \tag{66}$$

$$\begin{aligned}
T_{R0}(t) &= T_{R0e_2} + c_{11}\cos(\psi - \theta) + c_{12}a\cos\psi + c_{13}a^3\cos\psi + c_{14}a^2\cos(2\psi) + c_{15}a^3\cos(3\psi)\\
&+ c_{16}\sin(\psi - \theta) + c_{17}a\sin\psi + c_{18}a^3\sin\psi + c_{19}a^3\sin(3\psi) + c_{20}a^2\sin(2\psi)
\end{aligned} \tag{67}$$

$$\begin{aligned}
T_{R1}(t) &= c_{21}\cos(\psi - \theta) + c_{22}a\cos\psi + c_{23}a^3\cos\psi + c_{24}a^2\cos(2\psi) + c_{25}a^3\cos(3\psi)\\
&+ c_{26}\sin(\psi - \theta) + c_{27}a\sin\psi + c_{28}a^3\sin\psi + c_{29}a^2\sin(2\psi) + c_{30}a^3\sin(3\psi)
\end{aligned} \tag{68}$$

where $\psi = \Omega t + \theta$ and

$$
\begin{aligned}
&c_6 = \frac{\sqrt{a_{14}}}{2\sqrt{2}\Omega} - \frac{\sqrt{a_{14}}\sigma}{4\sqrt{2}\Omega^3}, c_7 = \frac{\sqrt{a_{14}^3}}{16\sqrt{2}\Omega^3}, c_8 = \frac{\sqrt{2}\sqrt{a_{14}}f}{3\Omega^3}, c_9 = \frac{a_{12}\sqrt{a_{14}}}{3\sqrt{2}\Omega^2}, c_{10} = \frac{a_{14}}{8\Omega^2},\\
&c_{11} = \frac{a_{22}^2 a_{24}\Omega f}{\sqrt{2}\sqrt{a_{14}}\left(a_{22}^2+\Omega^2\right)^2},\\
&c_{12} = -\frac{a_{24}\Omega\left(-a_{12}a_{22}^3 + a_{12}a_{22}\Omega^2 + 3a_{22}^2\sigma + 2a_{22}^2\Omega^2 + \sigma\Omega^2 + 2\Omega^4\right)}{2\sqrt{2}\sqrt{a_{14}}\left(a_{22}^2+\Omega^2\right)^2},\\
&c_{13} = \frac{\sqrt{a_{14}}a_{24}\Omega\left(17a_{22}^2+5\Omega^2\right)}{4\sqrt{2}\left(a_{22}^2+\Omega^2\right)^2}, c_{14} = -\frac{2a_{24}\Omega^2}{a_{22}^2+4\Omega^2}, c_{15} = -\frac{27\sqrt{a_{14}}a_{24}\Omega}{8\sqrt{2}\left(a_{22}^2+9\Omega^2\right)},\\
&c_{16} = -\frac{a_{22}a_{24}\left(a_{22}^2-\Omega^2\right)f}{2\sqrt{2}\sqrt{a_{14}}\left(a_{22}^2+\Omega^2\right)^2}, c_{17} = \frac{a_{22}a_{24}\left(a_{12}a_{22}\Omega^2 + a_{22}^2\left(\sigma+\Omega^2\right)+\Omega^4\right)}{\sqrt{2}\sqrt{a_{14}}\left(a_{22}^2+\Omega^2\right)^2},\\
&c_{18} = -\frac{\sqrt{a_{14}}a_{22}a_{24}\left(11a_{22}^2-\Omega^2\right)}{4\sqrt{2}\left(a_{22}^2+\Omega^2\right)^2}, c_{19} = \frac{9\sqrt{a_{14}}a_{22}a_{24}}{8\sqrt{2}\left(a_{22}^2+9\Omega^2\right)}, c_{20} = \frac{a_{22}a_{24}\Omega}{a_{22}^2+4\Omega^2},\\
&c_{21} = \frac{a_{32}^2 a_{33}f}{\left(a_{32}^2+\Omega^2\right)^2}, c_{22} = \frac{a_{33}\left(a_{12}a_{32}(a_{32}-\Omega)(a_{32}+\Omega) - 2\left(a_{32}^2\left(\sigma+\Omega^2\right)+\Omega^4\right)\right)}{2\left(a_{32}^2+\Omega^2\right)^2},\\
&c_{23} = \frac{3a_{14}a_{32}^2 a_{33}}{\left(a_{32}^2+\Omega^2\right)^2}, c_{24} = -\frac{\sqrt{2}\sqrt{a_{14}}a_{33}\Omega}{a_{32}^2+4\Omega^2}, c_{25} = -\frac{9a_{14}a_{33}}{8\left(a_{32}^2+9\Omega^2\right)},\\
&c_{26} = -\frac{a_{32}a_{33}(a_{32}-\Omega)(a_{32}+\Omega)f}{2\Omega\left(a_{32}^2+\Omega^2\right)^2}, c_{27} = \frac{a_{32}a_{33}\left(\Omega^2(2a_{32}(a_{12}+a_{32})-\sigma) + a_{32}^2\sigma + 2\Omega^4\right)}{2\Omega\left(a_{32}^2+\Omega^2\right)^2},\\
&c_{28} = \frac{3a_{14}a_{32}a_{33}\left(\Omega^2-a_{32}^2\right)}{2\Omega\left(a_{32}^2+\Omega^2\right)^2}, c_{29} = \frac{\sqrt{a_{14}}a_{32}a_{33}}{\sqrt{2}\left(a_{32}^2+4\Omega^2\right)}, c_{30} = \frac{3a_{14}a_{32}a_{33}}{8a_{32}^2\Omega + 72\Omega^3}
\end{aligned}
\tag{69}
$$

As alternative asymptotic procedure aimed at improving the description of the membrane temperature dynamics, resonance condition is imposed only to the terms related to W and W^2 in the mechanical equation (10). Using the same asymptotic scheme as the one previously described, the analytical response of the membrane temperature, which is formally identical to (67), shows different expressions of the following coefficients:

$$
\begin{aligned}
&c_{11} = -\frac{a_{17}a_{22}^2 a_{24}\omega}{\sqrt{2}\sqrt{a_{14}}\left(a_{22}^2+\Omega^2\right)^2},\\
&c_{12} = \frac{a_{24}\omega\left(a_{12}\left(a_{22}^3 - a_{22}\Omega^2\right) - 2\left(a_{22}^2\left(\sigma+\Omega^2\right)+\Omega^4\right)\right)}{2\sqrt{2}\sqrt{a_{14}}\left(a_{22}^2+\Omega^2\right)^2},\\
&c_{13} = \frac{\sqrt{a_{14}}a_{24}\left(a_{22}^2(12\omega+5\Omega)+5\Omega^3\right)}{4\sqrt{2}\left(a_{22}^2+\Omega^2\right)^2},\ c_{14} = -\frac{a_{24}\Omega(\omega+\Omega)}{a_{22}^2+4\Omega^2},\\
&c_{15} = -\frac{9\sqrt{a_{14}}a_{24}(\omega+2\Omega)}{8\sqrt{2}\left(a_{22}^2+9\Omega^2\right)},\ c_{16} = \frac{a_{17}a_{22}a_{24}\omega\left(a_{22}^2-\Omega^2\right)}{2\sqrt{2}\sqrt{a_{14}}\Omega\left(a_{22}^2+\Omega^2\right)^2},\\
&c_{17} = \frac{a_{22}a_{24}\omega\left(2a_{12}a_{22}\Omega^2 + a_{22}^2\left(\sigma+2\Omega^2\right) - \sigma\Omega^2 + 2\Omega^4\right)}{2\sqrt{2}\sqrt{a_{14}}\Omega\left(a_{22}^2+\Omega^2\right)^2},\\
&c_{18} = -\frac{\sqrt{a_{14}}a_{22}a_{24}\left(a_{22}^2(6\omega+5\Omega) + \Omega^2(5\Omega-6\omega)\right)}{4\sqrt{2}\Omega\left(a_{22}^2+\Omega^2\right)^2},\\
&c_{19} = \frac{3\sqrt{a_{14}}a_{22}a_{24}(\omega+2\Omega)}{8\sqrt{2}\Omega\left(a_{22}^2+9\Omega^2\right)},\ c_{20} = \frac{a_{22}a_{24}(\omega+\Omega)}{2\left(a_{22}^2+4\Omega^2\right)}
\end{aligned}
\tag{70}
$$

In turn, the coefficients of mechanical and bending thermal solutions are identical to those of the fully resonant asymptotic procedure, apart from a very minor difference. Thus they are not reported here, for the sake of brevity.

Appendix D Multiple Scale analysis around double-zero bifurcation

Analysis near the bifurcation point is performed by introducing fractional power series expansions to study Eq. (4). Accordingly, three time scales have been introduced, i.e., $T_0 = t$, $T_1 = \epsilon^{1/2}t$, $T_2 = \epsilon t$, and consistently, the time derivatives are expressed as

$$\begin{aligned} d/dt &= D_0 + \epsilon^{1/2} D_1 + \epsilon D_2 \\ d^2/dt^2 &= D_0^2 + 2\epsilon^{1/2} D_0 D_1 + \epsilon D_1^2 + 2\epsilon D_0 D_2 \end{aligned} \tag{71}$$

where $D_i = \partial/\partial T_i$. In order to account for the different time evolution of the mechanical variable with respect to the thermal ones, variables are scaled as follows:

$$\tilde{W} = \epsilon^{1/2}\, \hat{W}, \qquad \tilde{T}_{R0} = \epsilon\, \hat{T}_{R0}, \qquad \tilde{T}_{R1} = \epsilon\, \hat{T}_{R1} \tag{72}$$

so that their expression as perturbation of the reference equilibrium read:

$$\begin{aligned} \tilde{W}(t) &= \epsilon^{1/2} W_0(T_0,T_1,T_2) + \epsilon W_1(T_0,T_1,T_2) + \epsilon^{3/2} W_2(T_0,T_1,T_2) \\ \tilde{T}_{R0}(t) &= \epsilon T0_0(T_0,T_1,T_2) + \epsilon^{3/2} T0_1(T_0,T_1,T_2) + \epsilon^2 T0_2(T_0,T_1,T_2) \\ \tilde{T}_{R1}(t) &= \epsilon T1_0(T_0,T_1,T_2) + \epsilon^{3/2} T1_1(T_0,T_1,T_2) + \epsilon^2 T1_2(T_0,T_1,T_2) \end{aligned} \tag{73}$$

Since analysis is developed far from resonance regions (nonresonance condition), the forcing term is scaled to the generating order, i.e. $f = \epsilon^{1/2}\, \hat{f}$, while the other parameters are scaled as follows:

$$\omega^2 = \epsilon\, \hat{\omega}^2, \quad a_{12} = \epsilon\, \hat{a}_{12}, \quad a_{15} = \epsilon^{1/2}\, \hat{a}_{15}, \quad a_{33} = \epsilon^{1/2}\, \hat{a}_{33} \tag{74}$$

The resulting perturbation equations at each order read:

- Order ϵ
$$D_0^2 W_0 = f\cos(\Omega T_0) \tag{75}$$
- Order $\epsilon^{3/2}$
$$\begin{aligned} &D_0^2 W_1 = -2D_0 D_1 W_0 \\ &D_0 \mathrm{T}0_0 + a_{22}\mathrm{T}0_0 = -a_{24} W_0 D_0 W_0 \\ &D_0 \mathrm{T}1_0 + a_{32}\mathrm{T}1_0 = -a_{33} D_0 W_0 \end{aligned} \tag{76}$$
- Order ϵ^2
$$\begin{aligned} &D_0^2 W_2 = -\omega^2 W_0 - a_{14} W_0^3 - a_{12} D_0 W_0 - 2D_0 D_1 W_1 - D_1^2 W_0 \\ &- 2D_0 D_2 W_0 - a_{15}\mathrm{T}1_0 - a_{16}\mathrm{T}0_0 W_0 \\ &D_0 \mathrm{T}0_1 + a_{22}\mathrm{T}0_1 = -a_{24} W_0 D_0 W_1 - a_{24} W_0 D_1 W_0 - a_{24} W_1 D_0 W_0 - D_1 \mathrm{T}0_0 \\ &D_0 \mathrm{T}1_1 + a_{32}\mathrm{T}1_1 = -a_{33} D_0 W_1 - a_{33} D_1 W_0 - D_1 \mathrm{T}1_0 \end{aligned} \tag{77}$$

At first order, the solution of the mechanical equation (75) is combination of complementary and particular solution and reads

$$W_0 = A(T_1,T_2) - \frac{f}{2\Omega^2} \mathrm{e}^{i\Omega T_0} + c.c. \tag{78}$$

with $A(T_1,T_2)$ undetermined real amplitude which is function of the slow time scales, and $c.c.$ complex conjugate terms.

At order $\epsilon^{3/2}$, substituting W_0 in the first equation of (76) implies $D_0^2 W_1 = 0$, which furnishes null contribution to the modulation equation and to the mechanical solution, as well. In turn, solving the thermal equations yields the following particular solutions:

$$\begin{aligned} T0_0 &= -\frac{a_{24} f A \mathrm{e}^{i\Omega T_0}}{2ia_{22}\Omega - 2\Omega^2} - \frac{a_{24} f^2 \mathrm{e}^{2i\Omega T_0}}{4ia_{22}\Omega^3 - 8\Omega^4} + c.c. \\ T1_0 &= -\frac{a_{33} f \mathrm{e}^{i\Omega T_0}}{2ia_{32}\Omega - 2\Omega^2} + c.c. \end{aligned} \tag{79}$$

In view of Eqs. (78)-(79), the solvability condition of the mechanical problem at the order ϵ^2 (77) yields

$$D_1^2 A = c_1 A + c_3 A^3 \tag{80}$$

where

$$c_1 = -\omega^2 + \frac{3a_{14}f^2}{2\Omega^4} - \frac{2a_{16}a_{24}f^2}{4a_{22}^2\Omega^2 + 4\Omega^4},\ c_3 = -a_{14}$$

Moving to the real time scale t, the resulting amplitude modulation equation is

$$\ddot{A} = c_1 A + c_3 A^3 \tag{81}$$

Statements and Declarations

The authors declare that no funds, grants, or other support were received during the preparation of this manuscript.

The authors have no competing interests to declare that are relevant to the content of this article.

Data available on request from the authors.

References

1. J.J. McNamara and P.P. Friedmann. Aeroelastic and aerothermoelastic analysis in hypersonic flow: past, present, and future. *AIAA Journal*, 49(6):1089–1122, 2011.
2. P. Ribeiro. Thermally induced transitions to chaos in plate vibrations. *J. Sound Vib.*, 299(1):314–330, 2007.
3. P. Ribeiro and E. Jansen. Non-linear vibrations of laminated cylindrical shallow shells under thermomechanical loading. *J. Sound Vib.*, 315(3):626–640, 2008.
4. W. Zhang, J. Yang, and Y. Hao. Chaotic vibrations of an orthotropic FGM rectangular plate based on third-order shear deformation theory. *Nonlinear Dynam.*, 59(4):619–660, 2010.
5. F. Alijani, F. Bakhtiari-Nejad, and M. Amabili. Nonlinear vibrations of FGM rectangular plates in thermal enviroments. *Nonlinear Dynam.*, 66(3):251–270, 2011.
6. H.-S. Shen and Y. Xiang. Nonlinear vibration of nanotube-reinforced composite cylindrical panels,resting on elastic foundations in thermal environments. *Compos. Struct.*, 111:291–300, 2014.
7. K. Gao, W. Gao, D. Wu, and C. Song. Nonlinear dynamic characteristics and stability of composite orthotropic plate on elastic foundation under thermal environment. *Compos. Struct.*, 168:619–632, 2017.
8. P. Hong Cong, V.M. Anh, and N.D. Duc. Nonlinear dynamic response of eccentrically stiffened FGM plate using Reddy's TSDT in thermal environment. *J. Therm. Stresses*, 40(6):704–732, 2017.
9. N.V. Thanh, N.D. Khoa, N.D. Tuan, P. Tran, and N.D. Duc. Nonlinear dynamic response and vibration of functionally graded carbon nanotube-reinforced composite (FG-CNTRC) shear deformable plates with temperature-dependent material properties and surrounded on elastic foundations. *J. Therm. Stresses*, 40(10):1254–1274, 2017.

10. S. Yundong and W. Jian. Nonlinear response analysis and experimental verification for thin-walled plates to thermal-acoustic loads. *Chin. J. Aeronaut.*, 30(6):1919–1930, 2017.
11. E. Manoach, A. Warminska, J. Warminski, and S. Doneva. A reduced multimodal thermoelastic model of a circular mindlin plate. *Int. J. Mech. Sci.*, 153: 479–489, 2019.
12. E. Manoach, J. Warminski, L. Kloda, A. Warminska, and S. Doneva. Nonlinear vibrations of a bi-material beam under thermal and mechanical loadings. *Mech. Syst. Sig. Process.*, 177:109127, 2022.
13. R. Cukic. Coupled thermoelastic vibrations of plates. *Arch. Mech.*, 25:513, 1973.
14. W.P. Chang and S.M. Wan. Thermomechanically coupled nonlinear vibration of plates. *Int. J. Nonlinear Mech.*, 21(5):375–389, 1986.
15. X. Shu, X. Zhang, and J. Zhang. Thermoelastic free vibration of clamped circular plate. *Appl. Math. Mech.*, 21(6):715–724, 2000.
16. Y.-L. Yeh, C.-K. Chen, and H.-Y. Lai. Chaotic and bifurcation dynamic for a simply supported rectangular plate with thermo-mechanical coupling in large deflection. *Chaos Soliton Fract.*, 13(7):1493–1506, 2002.
17. Y.-L. Yeh. Chaotic and bifurcation dynamic behavior of a simply supported rectangular orthotropic plate with thermomechanical coupling. *Chaos Soliton Fract.*, 24(5):1243–1255, 2005.
18. Y.-L. Yeh. The effect of thermo-mechanical coupling for a simply supported orthotropic rectangular plate on non-linear dynamics. *Thin wall. Struct.*, 43 (8):1277–1295, 2005.
19. A.J. Culler and J.J. McNamara. Studies on fluid-thermal-structural coupling for aerothermoelasticity in hypersonic flow. *AIAA Journal*, 48(8):1721–1738, 2010.
20. A.J. Culler and J.J. McNamara. Impact of fluid-thermal-structural coupling on response prediction of hypersonic skin panels. *AIAA Journal*, 49(11):2393–2406, 2011.
21. E. Saetta and G. Rega. Unified 2D continuous and reduced order modeling of thermomechanically coupled laminated plate for nonlinear vibrations. *Meccanica*, 49(8):1723–1749, 2014.
22. E. Saetta and G. Rega. Third-order thermomechanically coupled laminated plates: 2D nonlinear modeling, minimal reduction and transient/post-buckled dynamics under different thermal excitations. *Compos. Struct.*, 174:420–441, 2017.
23. V. Settimi, G. Rega, and E. Saetta. Avoiding/inducing dynamic buckling in a thermomechanically coupled plate: a local and global analysis of slow/fast response. *Proc. R. Soc. London, Ser. A*, 474(2213):20180206, 2018.
24. G. Rega, E. Saetta, and V. Settimi. Modeling and nonlinear dynamics of thermomechanically coupled composite plates. *Int. J. Mech. Sci.*, 187:106106, 2020.
25. V. Settimi and G. Rega. Thermomechanical coupling and transient to steady global dynamics of orthotropic plates. In *Problems of Nonlinear Mechanics and Physics of Materials*, pages 483–499. Springer, 2019.
26. V. Settimi, E. Saetta, and G. Rega. Nonlinear dynamics of a third-order reduced model of thermomechanically coupled plate under different thermal excitations. *Meccanica*, 55(12):2451–2473, 2020.

27. A. H. Nayfeh and D. T. Mook. *Nonlinear oscillations*. John Wiley & Sons, 1979.
28. J. Awrejcewicz, R. Starosta, and G. Sypniewska-Kamińska. *Asymptotic Multiple Scale Method in Time Domain: Multi-Degree-of-Freedom Stationary and Non-stationary Dynamics*. CRC Press, 2022.
29. R.H. Rand, A.T. Zehnder, B. Shayak, and A. Bhaskar. Simplified model and analysis of a pair of coupled thermo-optical MEMS oscillators. *Nonlinear Dynam.*, 99(1):73–83, 2020.
30. S. Jain and P. Tiso. Model order reduction for temperature-dependent nonlinear mechanical systems: a multiple scales approach. *J. Sound Vib.*, 465:115022, 2020.
31. E.J. Doedel and B.E. Oldeman. *AUTO-07p: Continuation and bifurcation software for ordinary differential equations*. Concordia University, Montreal, 2012.
32. E. Saetta, V. Settimi, and G. Rega. Minimal thermal modeling of two-way thermomechanically coupled plates for nonlinear dynamics investigation. *J. Therm. Stresses*, 43(3):345–371, 2020.
33. Wolfram Research, Inc. Mathematica, Version 13.0.0, 2021. URL `https://www.wolfram.com/mathematica`. Champaign, IL.
34. A. Luongo and A. Di Egidio. Divergence, Hopf and double-zero bifurcations of a nonlinear planar beam. *Comput. Struct*, 84(24-25):1596–1605, 2006.
35. A. Luongo and D. Zulli. A paradigmatic system to study the transition from zero/Hopf to double-zero/Hopf bifurcation. *Nonlinear Dynam.*, 70(1):111–124, 2012.
36. S. Brischetto and E. Carrera. Coupled thermo-mechanical analysis of one-layered and multilayered plates. *Compos. Struct.*, 92(8):1793–1812, 2010.
37. A. Luongo and A. Paolone. On the reconstitution problem in the multiple time-scale method. *Nonlinear Dynam.*, 19(2):135–158, 1999.